# Discovery of Cyclic Sulfone Hydroxyethylamines as Potent and Selective β-Site APP-Cleaving Enzyme 1 (BACE1) Inhibitors: Structure-Based Design and in Vivo Reduction of Amyloid β-Peptides

Heinrich Rueeger,*,[†] Rainer Lueoend,[†] Olivier Rogel,[†] Jean-Michel Rondeau,[‡] Henrik Möbitz,[†] Rainer Machauer,[†] Laura Jacobson,[§] Matthias Staufenbiel,[§] Sandrine Desrayaud,[‖] and Ulf Neumann[§]

[†]Department of Global Discovery Chemistry, [‡]Structural Biology Platform, [§]Department of Neuroscience, and [‖]Metabolism and Pharmacokinetics, Institutes for BioMedical Research, Novartis Pharma AG, CH-4057 Basel, Switzerland

**S** *Supporting Information*

**ABSTRACT:** Structure-based design of a series of cyclic hydroxyethylamine BACE1 inhibitors allowed the rational incorporation of prime- and nonprime-side fragments to a central core template without any amide functionality. The core scaffold selection and the structure–activity relationship development were supported by molecular modeling studies and by X-ray analysis of BACE1 complexes with various ligands to expedite the optimization of the series. The direct extension from P1-aryl- and heteroaryl moieties into the S3 binding pocket allowed the enhancement of potency and selectivity over cathepsin D. Restraining the design and synthesis of compounds to a physicochemical property space consistent with central nervous system drugs led to inhibitors with improved blood–brain barrier permeability. Guided by structure-based optimization, we were able to obtain highly potent compounds such as **60p** with enzymatic and cellular $IC_{50}$ values of 2 and 50 nM, respectively, and with >200-fold selectivity over cathepsin D. Pharmacodynamic studies in APP51/16 transgenic mice at oral doses of 180 μmol/kg demonstrated significant reduction of brain Aβ levels.
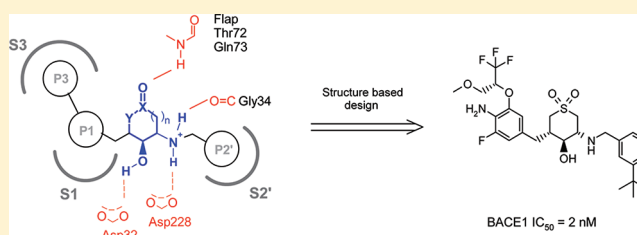
## INTRODUCTION

Alzheimer's disease (AD) is one of the most prevalent neurodegenerative disorders among the elderly and constitutes a considerable unmet medical need. Clinically, AD starts with minor episodic memory problems but progresses to major cognitive dysfunction accompanied by behavioral and neuropsychiatric disturbances. The disease dramatically affects daily living and leads to death about 8–9 years after diagnosis.[1] Pathological hallmarks of AD are neuritic plaques containing aggregated amyloid-β (Aβ) peptides as the core component and neurofibrillar tangles of aggregated τ protein. Considerable evidence has accumulated indicating a central role of the Aβ peptide and more specifically its aggregation in the pathogenesis of AD.[2]

Aβ is generated in the β-secretase pathway from the large transmembrane β-amyloid precursor protein (APP). The membrane-bound aspartic protease BACE1 (EC 3.4.23.46) initiates the pathway by cleaving APP at position one of Aβ,[3-7] generating the secreted amino-terminal part of APP (sAPPβ) as well as the carboxy-terminal fragment C99. This transmembrane fragment is further cleaved by γ-secretase leading to Aβ.[8,9] An alternative but less frequent BACE1 cleavage at position 11 of Aβ generates a shorter carboxy-terminal fragment, C89, and an Aβ fragment starting at amino acid 11.[10-12] Cleavage at this site was shown to reduce Aβ generation.[13] APP may also be processed via the α-secretory pathway, which is initiated by α-secretase cleavage in the center of Aβ leading to sAPPα and C83. The carboxy-terminal fragment is also cleaved by γ-secretase, resulting in P3, a peptide starting at amino acid 17.

Knockout of the BACE1 gene blocks not only the generation of Aβ but also that of C99.[14-19] In addition, APP processing shifts toward the α-secretory pathway as indicated by an increase in sAPPα and C83. Interestingly, mice carrying only a single BACE1 allele showed a 50% reduction in BACE1 enzyme activity but a much smaller effect on Aβ.[16,19-23] These data indicate that BACE1 is in excess over APP at the cleavage site(s) and that Aβ lowering might require an overproportional reduction in enzyme activity. On the other hand, a moderate 12% Aβ decrease in APP transgenic mice with a single BACE1 allele translated into a pronounced (70–90%) reduction of amyloid deposition.[22] Toxic Aβ aggregates may, therefore, be especially sensitive to Aβ lowering.

BACE1 knockout disturbs postnatal neuregulin 1 (NRG1) processing, resulting in hypomyelination,[23-25] whereas no differences in brain NRG1 processing were found in mature and aged animals.[23] Both a delay in remyelination and enhanced regeneration after injury have been described.[26,27] Alterations in neuronal activity were also noted in BACE1

deficient mice.[28,29] While the relevance of these observations to BACE1 reduction in the adult remains unclear, general and consistent toxicity was not observed in mice lacking BACE1 activity. The inhibition of BACE1, therefore, is an attractive approach for the development of causal AD therapies.

BACE1 belongs to the aspartyl protease family with two aspartic acids constituting the catalytic diad in the center of a large binding site extending over 6–8 amino acid residues. There are significant challenges in designing potent, selective, and brain penetrant BACE1 inhibitors.[30] Standard high-throughput screening (HTS) methods failed in many institutions to deliver hits for hit to lead optimization. Most of the initial lead compounds have been generated by rational structure-based design of peptidomimetics. Traditional substrate-based statine, homostatine, and hydroxyethylene (HE) peptide transition state (TS) mimetics were selected for a structure-based optimization, resulting in highly potent inhibitors as represented by OM99-2 (Figure 1, IC$_{50}$ = 2 nM).[31]
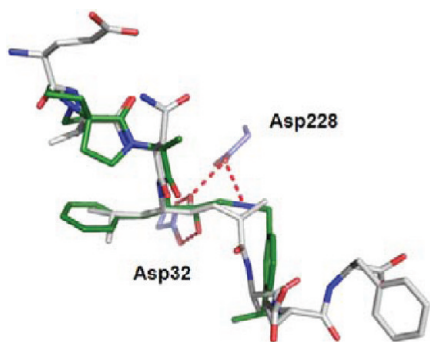


**Figure 1.** Superposition of HE isostere inhibitor OM99-2 (gray; PDB code: 1fkn) with hydroxyethylamine dipeptide isostere inhibitor **3** (green).

The HE TS mimetic was soon surpassed by the more cell-permeable hydroxyethylamine (HEA) TS mimetic (Figure 2) requiring the opposite stereochemistry at the hydroxyl group as represented by **1** (IC$_{50}$ = 20 nM),[32,38a] the further optimized analogue **2** (IC$_{50}$ = 47 nM),[33,34] and our initial acyclic HEA lead compound **3** (IC$_{50}$ = 55 nM).[35]

However, the major drawback of most of these very potent initial HEA BACE1 inhibitors is their high molecular weight (MW > 450), their high conformational flexibility, and the numerous subsite interactions along the native peptide

backbone extending from P3 to P2′. In addition, the individual subsites are linked by amide groups providing both hydrogen bond donors (HBD) and/or acceptors (HBA) at positions that are well recognized by the P-glycoprotein transporter (P-gp), therefore limiting their ability to cross the blood–brain barrier (BBB).[36] Over the years, a multitude of HEA inhibitors have been designed and optimized in different research laboratories,[37,38] and a detailed understanding of the enzyme–HEA inhibitor interactions spanning the S3 to S2′ binding pockets became available. Unfortunately, the majority of these peptidomimetic inhibitors displayed a poor oral bioavailability and/or a limited penetration into the brain parenchyma, both resulting in a lack of effect on Aβ in pharmacodynamic (PD) models in rodents. These exposure liabilities were due to extensive metabolic clearance, insufficient permeability, and P-gp-mediated efflux at the BBB. In recent years, there has been a growing interest in identifying novel TS mimetics by HTS at high concentrations (>30 μM) and fragment-based screening (FBS) to evade the poor property space of peptidomimetic BACE1 inhibitors.[37,39,40] At the outset of our efforts, there were no BACE1 inhibitors known to reduce Aβ$_{40/42}$ formation in the brain. However, within the past few years, a few compounds appeared in the literature that could demonstrate high in vitro activity and significant brain Aβ reduction in different animal PD models.[38o,39g–k,40g]

Previously, we reported our research concerning the identification of a novel class of brain-penetrating cyclic hydroxyethylamine (cHEA) BACE1 inhibitors by a de novo design approach.[41] Herein, we describe the design, synthesis, and optimization efforts to improve potency, cellular activity, selectivity over cathepsin D (CatD), and pharmacokinetic properties of the initial cHEA inhibitor **4** (Figure 3).
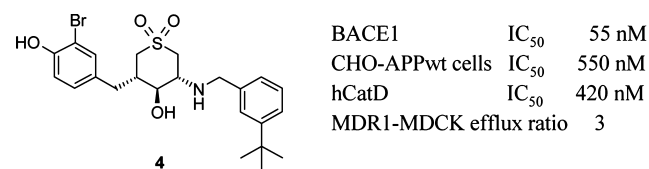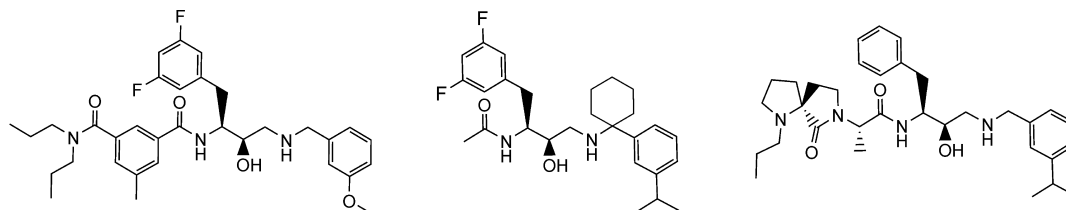


| BACE1 | IC$_{50}$ | 55 nM |
| CHO-APPwt cells | IC$_{50}$ | 550 nM |
| hCatD | IC$_{50}$ | 420 nM |
| MDR1-MDCK efflux ratio | | 3 |

**Figure 3.** Sulfone cHEA inhibitor **4**.

**Inhibitor Design Concept.** To improve the pharmacokinetic and brain penetration properties for this challenging drug target, we decided to eliminate the amide functionalities of the peptide backbone. To reduce the rather high flexibility of acyclic HEA TS mimetics, the essential HEA TS mimetic was



| | **1**[32] | **2**[33,34] | **3**[35] |
|---|---|---|---|
| BACE1 IC$_{50}$ | 20 nM[38a] | 47 nM | 55 nM |
| APP HEK293 cell IC$_{50}$ | 15 nM[38a] | 17 nM | 10 nM |
| P$_{app}$ in MDR1-MDCK cells | n.a. | 7 nm/s | 110 nm/s |
| MDR1-MDCK efflux ratio | n.a. | 19-fold | 23-fold |

**Figure 2.** Representative HEA TSM BACE1 inhibitors. Compounds are strong P-gp substrates based on the MDR1-MDCK permeability assay.

embedded into a cyclic TS mimetic (cHEA), retaining the essential H-bonding interactions with the aspartyl protease catalytic diad and the flap. In addition, the cyclic scaffold should provide suitable attachment vectors for direct extensions into the corresponding S2′- and S1/S3 subsites (Figure 4). This
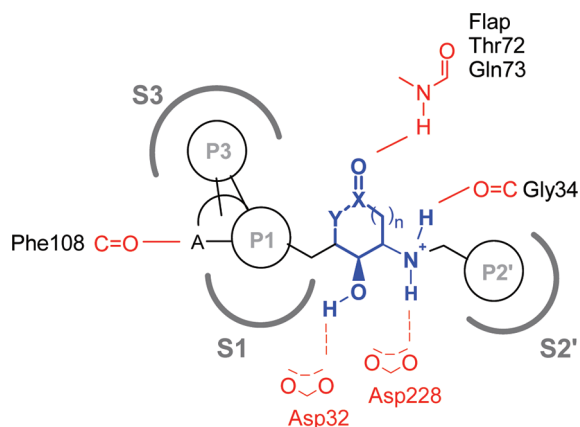


**Figure 4.** Envisaged binding mode for P3−P1 subsite-linked cHEA inhibitors. A represents a H-bond donor group; X = C, S; Y = C, N; and *n* = 0, 1, or 2.

design concept should provide inhibitors with improved BBB permeability, due to their lower polar surface area (PSA) and decreased susceptibility to P-gp-induced efflux.

Selectivity over CatD is highly desired, since CatD deficiency is related to neuronal ceroid lipofuscinosis in animal models and in humans.[42] To enhance the selectivity against CatD, the individual binding sites were examined for differentiation in hydrophobic contacts and H-bonding interactions. Full occupancy of the BACE1 S1−S3 pocket should result in some steric clashes in the slightly smaller CatD S1−S3 binding pocket. The utilization of a H-bonding interaction to BACE1 Phe108, which cannot be formed in CatD, should lead to an increase in selectivity by gain of BACE1 potency (Figure 4 and cocrystal structure of initial lead with BACE1 in Figure 6).

To achieve a good brain penetration [assessed by the in vivo brain/blood concentration ratio and the in vitro permeability and efflux ratio (ER) through a MDR1-MDCK cell monolayer], special attention has to be paid to the physicochemical parameters during lead optimization. For instance, a moderate-to-high permeability (>150 nm/s) commonly observed for central nervous system (CNS) drugs has to be attained.[43] Remaining within the boundaries of CNS drugs property space already during the structure-based design [MW < 450 Da, PSA < 75 Å, clog *P* < 4, number of oxygen and nitrogen atoms $\sum(N + O) < 5$],[44a,b] and p$K_a$ <8 to minimize P-gp[38l,n] and hERG channel interactions,[45] should lead to drug candidates with improved pharmacokinetic and safety profiles. With these constraints in mind and relying on a highly conserved binding mode for HEA inhibitors,[46] cHEA TS mimetics were designed, and P3−P1 and P2′ fragments extending into the S1−S3 and S2′ pockets, respectively, were optimized.

**Identification of Initial Candidates.** In an iterative process, a diverse set of 5−7 membered scaffolds with an embedded HEA moiety and attached P1 and P2′ fragments were docked using QXP with the Flo modeling package.[47] Conformational energy, S3, S1, S1′, and S2′ site occupancy, and the overall binding potential were assessed, including key H-

bonding interactions to the catalytic residues Asp32 and Asp228, to the flap residues Gln73 and Thr72, and to Gly34 and Phe108. Connections and subsite fragments were modified and redocked again until inhibitor candidates within the desired property space and binding profile were identified. For the identified matured candidates **A**−**D** (Figure 5), a synthesis had
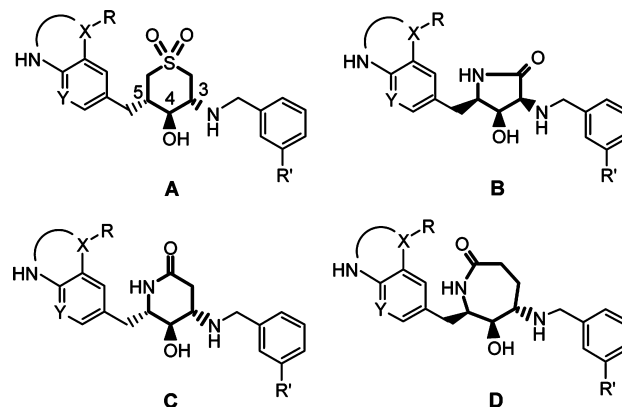


**Figure 5.** Matured candidate cHEA TS mimetics generated by de novo design.

to be generated, which presents an additional effort in comparison to hits identified by a HTS or FBS campaign, before their activity could be measured and the binding mode assessed by cocrystallization with BACE1.

Candidate **A** containing a sulfone cHEA TS mimetic, whose 1,1-dioxo-tetrahydro-thiopyran-4-ol core scaffold is amino substituted at C-3, amenable for facile prime side pharmacophore optimization, and tethered at C-5 to the P3−P1 pharmacophore by a benzylic moiety, generated the best ranking pose. The docking of the 5-, 6-, and 7-membered lactam cHEA TS mimetics **B**, **C**, and **D** produced a less optimal fit. Their synthetic exploitation was considered to be more cumbersome as compared to scaffold **A**, which presented all substitutions on the cHEA scaffold in the energetically favored equatorial conformation, while the SO$_2$ group projected optimal H-bonding interactions to Gln73 and Thr72 of the flap. To further improve potency, selectivity and metabolic stability of the initial P1 3-bromo-4-hydroxybenzyl-substituted sulfone cHEA inhibitor **4**, different aryl and heteroaryl P3−P1 fragments were generated by structure-based design.

## ■ CHEMISTRY

As outlined in Scheme 1, we selected a synthetic approach whereby we first assembled the core disubstituted tetrahydro-thiopyranone scaffold **E** from N- and S-protected cysteine **5**. The previously described approach,[41] via a Dieckmann condensation followed by multiple functional group manipulations, including a Curtius rearrangement to generate 3-substituted 4-hydroxybenzyl-extended sulfone cHEA inhibitors, could not be applied to different (P3)-P1-substituted aldehydes. Several attempts to directly functionalize the tetrahydro-thiopyran-4-one **6** were not very promising. Because ketone-enolate alkylations on **6** proved to be difficult, we switched to the keto-ester intermediate **E**, which would allow the alkylation of a wide variety of benzylic P3−P1 fragments under mild conditions. Subsequent decarboxylation, stereoselective ketone reduction, oxidation to the sulfone, and ultimate prime side extension by reductive amination should

**Scheme 1. Retro-Synthetic Analysis of Candidate A Type cHEA Inhibitors**
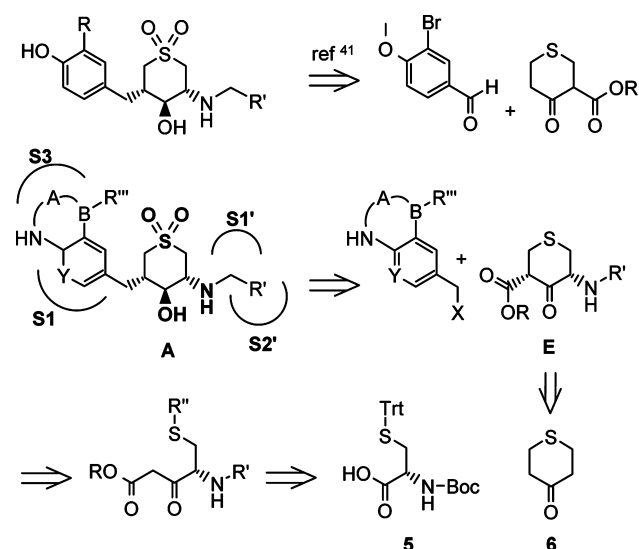


allow diverse prime and nonprime side structure–activity relationship (SAR) exploration (see also Scheme 3).

**Synthesis of the Tetrahydro-thiopyranone Core Scaffold E (8).** The synthesis of the *N*-Boc $\beta$-keto-allylester intermediate **8** is shown in Scheme 2. The *N*-Boc- and *S*-trityl-

**Scheme 2. Synthesis of the *N*-Boc $\beta$-Keto-allylester Intermediate 8 (Scaffold E)**[a]
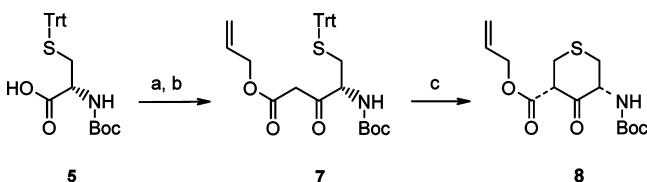


[a]Reagents and conditions: (a) Carbonyldiimidazole, 4-(*N,N*-dimethylamino)pyridine, THF, 25 °C. (b) Propanedioic acid, mono-2-propenyl ester, magnesium complex, THF, 45 °C. (c) *para*-Formaldehyde, piperidine, acetic acid, 80 °C.

protected (*S*)-cysteine **5** was transformed under standard conditions into the corresponding allylic keto-ester **7** by treatment with carbonyldiimidazole followed by the addition of propanedioic acid mono-2-propenyl ester magnesium complex in tetrahydrofuran (THF). Condensation of the keto-ester **7** with *para*-formaldehyde in acetic acid was performed at 80 °C to facilitate in situ dehydration. Deprotection of the thiol group and intramolecular Michael addition in a single step cleanly delivered the *N*-Boc-protected keto-ester intermediate **8**. Upon recrystallization, the pure *cis* isomer could be obtained. However, under the above reaction conditions, the amino substituent had fully racemized.

**Synthesis of P1-Substituted Benzyl Sulfone cHEA Inhibitors.** Scheme 3 describes the synthesis of 4-amino-3-fluoro-benzyl cHEA inhibitors **14** and **15**. The central intermediate **13** used for the exploration of the P3 pocket was prepared from *N*-Boc $\beta$-keto-allylester **8** (Scheme 2), a suitable cHEA building block for tethering structurally different P3–P1 fragments, and the commercially available 1-bromo-methyl-4-nitro-benzene. The commonly used multistep sequence started with the alkylation of an activated benzylic P1
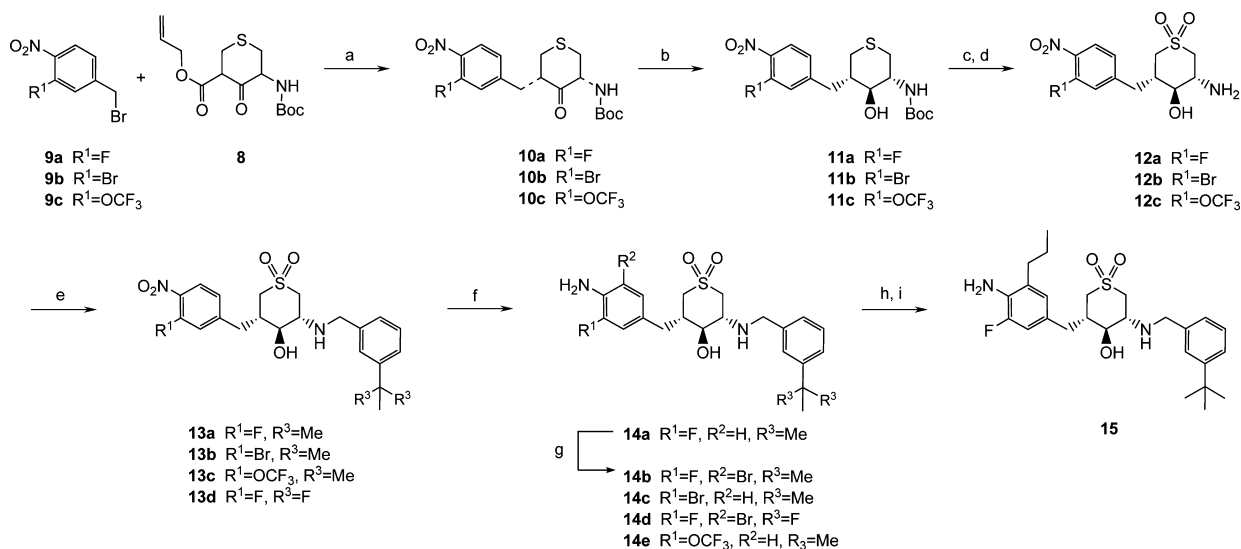
fragment like **9** under mild conditions ($K_2CO_3$ in acetone at 25−50 °C) followed by Pd-catalyzed allyl-ester cleavage and spontaneous decarboxylation to generate the *N*-Boc ketone intermediate, which upon 1,8-diazabicycloundec-7-ene (DBU)-catalyzed equilibration in THF afforded almost exclusively the thermodynamically more stable *cis-N*-Boc ketone **10**. Reduction with LiAlH$_4$ at low temperature provided the desired (3*R**,4*S**,5*S**)-diastereoisomer of the 5-substituted 3-amino-tetrahydro-thiopyran-4-ol **11** with moderate diastereoselectivity (5:1). Enantiopure material could be best obtained by chiral HPLC separation at this stage. The following potassium peroxomonosulfate oxidation yielded a less soluble *N*-Boc-protected sulfone intermediate. Final *N*-Boc deprotection with 4 N HCl in dioxane afforded the P1-substituted cHEA **12**, set for an efficient elaboration of the P2′ SAR, as exemplified by the reductive amination with 3-*tert*-butyl-benzaldehyde to the prime side-substituted cHEA **13**. Direct reduction of the nitro group with nickel-borohydride gave the 4-amino-3-fluoro-aryl inhibitor **14a**. The synthesis of the 4-amino-3-bromo-5-fluoro-aryl derivative **14b** was completed by bromination of **14a** with 1,3-di-*n*-butylimidazolium tribromide. Suzuki coupling of **14b** with 2-allyl-4,4,5,5-tetramethyl[1,3,2]dioxaborolane followed by catalytic hydrogenation of the olefin afforded the 4-amino-3-fluoro-5-*n*-propyl-benzyl inhibitor **15**.

**Synthesis of P1 Heteroaryl-methyl-Substituted Sulfone cHEA Inhibitor 18.** The P1 amino-pyridine-substituted cHEA inhibitor **18** was prepared according to Scheme 4. The *N*-benzyloxycarbonyl-protected 5-bromomethyl-pyridin-2-yl-amine **17** was prepared from 6-amino-nicotinic acid methyl ester **16** by reduction with LiAlH$_4$ in THF to the benzylic alcohol and conversion into the benzyl bromide **17** with CBr$_4$–PPh$_3$. The attachment of **17** to the central cHEA building block **8** and the transformation into the final amino-pyridine-substituted inhibitor **18** was accomplished using the same procedures used to prepare inhibitor **14a** (Scheme 3).

**Synthesis of P3−P1 Bicyclic Heteroaryl-methyl-Substituted Sulfone cHEA Inhibitors.** The indazole inhibitor **22** was synthesized from 5-bromomethyl-indazole **19** (Scheme 5) and **8** using the same general procedure as for the cHEA inhibitor **14a**. For the *n*-propyl P3-extended analogue **24**, the indazole intermediate **21** was brominated at C-3 with *N*-bromosuccinimide, and the indazole was *tert*-butyloxycarbonyl protected for the Pd-catalyzed C-3 alkylation with 2-allyl-4,4,5,5-tetramethyl-1,2,3-dioxa-borolane. Catalytic hydrogenation of the olefin, *N*-Boc deprotection with 4 N HCl in dioxane, and subsequent reductive amination using the procedure as for **15** provided the 3-substituted indazole inhibitor **24**.

The synthesis of the 3-unsubstituted indole inhibitor **27** was carried out as shown in Scheme 6. The *N*-phenylsulfonyl-protected 5-indole carboxylic acid methyl ester **25** was reduced with diisobutylaluminium hydride in THF to the benzylic alcohol, which after conversion to the benzyl bromide **26** was transformed into the indole-containing inhibitor **27** by the same reaction sequence as applied previously for the cHEA inhibitor **15**.

The 3-difluoroethyl-substituted indole **32a** was prepared according to Scheme 7. *N*-Tosyl-protected 5-bromoindole **28** was acylated with difluoroacetic acid anhydride and AlCl$_3$ in CH$_2$Cl$_2$. Reduction of the difluoroketone to the 3-difluoroethyl-substituted indole **29** with BH$_3$-THF was only successful after intermediate N-deprotection. The transformation of **29** into the benzyl bromide **30** was accomplished by a multistep reaction sequence, initiated by a Pd-catalyzed vinylation at C-5

**Scheme 3. Synthesis of P1-Substituted Benzyl Sulfone cHEA Inhibitors 14a–e and 15**[a]



9a R[1]=F
9b R[1]=Br
9c R[1]=OCF₃

10a R[1]=F
10b R[1]=Br
10c R[1]=OCF₃

11a R[1]=F
11b R[1]=Br
11c R[1]=OCF₃

12a R[1]=F
12b R[1]=Br
12c R[1]=OCF₃

13a R[1]=F, R[3]=Me
13b R[1]=Br, R[3]=Me
13c R[1]=OCF₃, R[3]=Me
13d R[1]=F, R[3]=F

14a R[1]=F, R[2]=H, R[3]=Me
14b R[1]=F, R[2]=Br, R[3]=Me
14c R[1]=Br, R[2]=H, R[3]=Me
14d R[1]=F, R[2]=Br, R[3]=F
14e R[1]=OCF₃, R[2]=H, R₃=Me

15

[a]Reagents and conditions: (a) (i) K₂CO₃, acetone, 25–50 °C; (ii) Pd(PPh₃)₄, morpholine, THF; (iii) cat. DBU, THF, 25 °C. (b) (i) LiAlH₄, THF, −70 °C; (ii) separation by preparative HPLC on Chiralpak AD-I (hexane–CH₂Cl₂–iPrOH–EtOH 75:20:2.5:2.5), >98% ee. (c) Potassium peroxomonosulfate, THF–H₂O 1:1, 25 °C. (d) 4 N HCl in dioxane, 25 °C. (e) (i) 3-*tert*-Butyl-benzaldehyde, NaOAc, MeOH–CH₂Cl₂ 1:1, 25 °C; (ii) NaBH₃CN, MeOH, 25 °C. (f) NiCl₂–6H₂O, NaBH₄, MeOH, 0 °C. (g) 1,3-Di-*n*-butylimidazolium tribromide, CH₂Cl₂, −10 °C. (h) 2-Allyl-4,4,5,5-tetramethyl[1,3,2]dioxaborolane, Pd₂(dba)₃, 1,2,3,4,5-pentaphenyl-1-(di-*t*-butylphosphino)-ferrocene, K₃PO₄, DME–H₂O, 80 °C. (i) H₂, 10% Pd–C, MeOH, 25 °C.

**Scheme 4. Synthesis of P1 Heteroaryl-methyl-Substituted Inhibitor 18**[a]



16

17

18
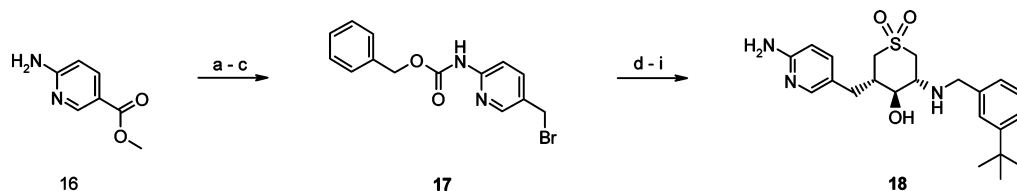
[a]Reagents and conditions: (a) Benzyl chloroformate, NaHCO₃, ethylacetate–H₂O, 25 °C. (b) LiAlH₄, THF, 0 °C. (c) CBr₄, triphenylphosphine, CH₂Cl₂, 0 °C. (d) (i) Compound **8**, K₂CO₃, acetone, 25 °C; (ii) Pd(PPh₃)₄, morpholine, THF; (iii) cat. DBU, THF, 25 °C. (e) (i) LiAlH₄, THF, −40 °C. (f) Potassium peroxomonosulfate, THF–H₂O 1:1, 25 °C. (g) 4 N HCl in dioxane, 25 °C. (h) (i) 3-*tert*-Butyl-benzaldehyde, NaOAc, MeOH–CH₂Cl₂ 1:1, 25 °C, (ii) NaBH₃CN, MeOH, 25 °C. (i) H₂, 10% Pd–C, MeOH, 25 °C.

with potassium vinyl tetrafluoroborate, OsO₄-catalyzed oxidative cleavage of the double bond to the aldehyde, followed by NaBH₄ reduction to the benzylic alcohol and conversion into the benzyl bromide with PBr₃. Subsequent transformation into the 3-difluoromethyl-indole inhibitor **32a** was accomplished in a similar fashion via *N*-Boc intermediate **31** as previously described for inhibitor **14a**.

The synthesis of the spiro-indoline inhibitors **39a** and **39b** was carried out as exemplified for **39a** in Scheme 8. The 7-fluoroindoline-2,3-dione **33** was reduced with hydrazine and converted to the spiro-ketone **34** by a double Michael addition, Dieckmann condensation, and decarboxylation sequence in a single step with ethyl-acrylate. The gem-difluoro derivative **35** was prepared via the ketoxime under mild conditions using a modified procedure developed by Olah[48] to minimize olefin formation. The transformation of the arylbromide **35** into the benzyl alcohol **36** was accomplished by Pd-catalyzed vinylation with potassium vinyl tetrafluoroborate followed by ozonolysis of the olefine and in situ NaBH₄ reduction of the ozonide. Subsequent attachment of the benzyl alcohol **36** to the ketoester **8** was carried out under Mitsunobu conditions, and the conversion of **37** into inhibitor **39a** was accomplished in a

similar fashion via the *N*-Boc intermediate **38** as previously described for inhibitor **14a**.
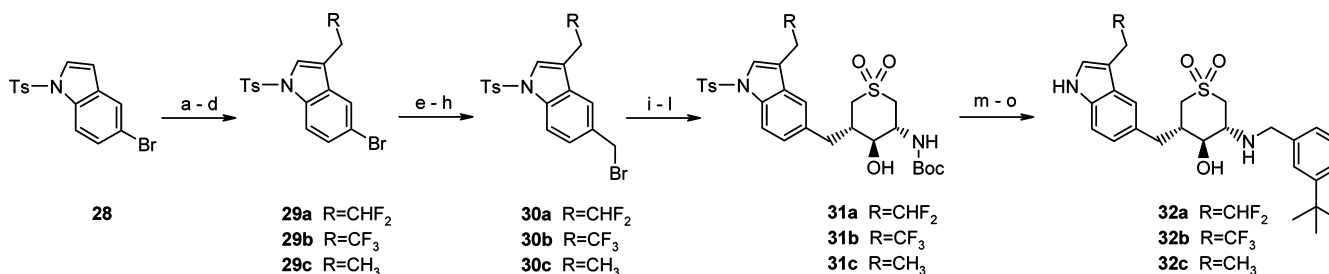
**Synthesis of P3 Alkyl-Substituted Benzyl Sulfone cHEA Inhibitors.** The 5-alkyl-substituted benzyl sulfone cHEA inhibitors **41a,b** in Table 4 were prepared according to Scheme 9. The amino-alcohol **13a** (Scheme 3) was first converted into oxazolidinone **40** with carbonyldiimidazole, followed by substitution of the fluorine with the corresponding alcohol under basic conditions. Hydrolysis of the oxazolidinone with Ba(OH)₂ and catalytic reduction of the nitro group with Pd–C in THF afforded **41a** and **41b**. The N-acylated derivative **42** was obtained from oxazolidinone **40** by catalytic hydrogenation of the nitro group followed by acylation of the aniline and hydrolysis of the oxazolidinone under mild conditions with potassium trimethylsilanolate in THF at 50 °C. The P3 extended analogues **44−47** were synthesized via the more reactive oxazolidinone-protected aryl-iodide **43** by Suzuki coupling with the corresponding boronic acids followed by the same deprotection procedures as described for **42**. In the case of the trifluoropropyl P3 extension, the CF₃C≡CZnCl reagent[49] was prepared for the Pd-catalyzed coupling. The 2-hydroxylated trifluoropropyl analogue **48** was synthesized from **43** by *N*,*N*-dimethyl-formamidine protection of the aniline

## Scheme 5. Synthesis of Indazole Inhibitors 22 and 24[a]
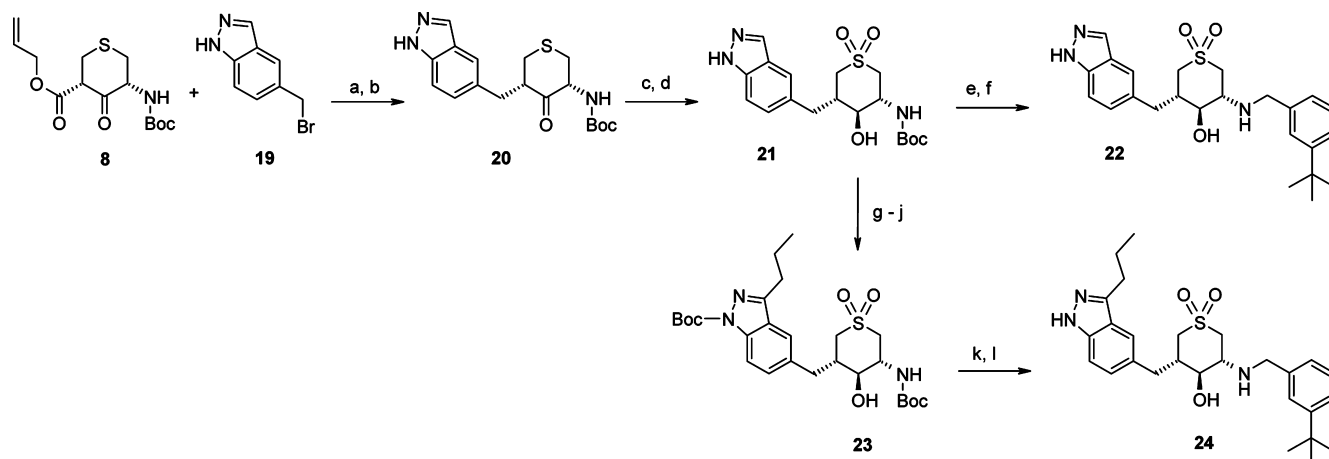


[a]Reagents and conditions: (a) $K_2CO_3$, acetone, 25 °C. (b) (i) Pd(PPh$_3$)$_4$, morpholine, THF, 25 °C; (ii) cat. 1,8-diazabicyclo[5.4.0]undec-7-ene, THF, 25 °C. (c) LiAlH$_4$, THF, −60 °C. (d) Potassium peroxomonosulfate, THF−H$_2$O 1:1, 25 °C. (e) 5 N HCl in $i$-PrOH, 25 °C. (f) (i) 3-$tert$-Butyl-benzaldehyde, NaOAc, MeOH−CH$_2$Cl$_2$ 1:1, 25 °C. (ii) NaBH$_3$CN, MeOH, 25 °C. (g) $N$-Bromosuccinimide, acetonitrile, 25 °C. (h) Di-$t$-butyl dicarbonate, triethylamine, acetonitrile, 25 °C. (i) 2-Allyl-4,5,5-tetramethyl-1,2,3-dioxa-borolane, Pd$_2$(dba)$_3$, 1,2,3,4,5-pentaphenyl-1′-(di-$tert$-butylphosphino)ferrocene, K$_3$PO$_4$, DME/H$_2$O 10:1, 85 °C. (j) H$_2$, 10% Pd−C, MeOH, 25 °C. (k) 4 N HCl in dioxane, 25 °C. (l) (i) 3-$tert$-Butyl-benzaldehyde, NaOAc, MeOH−CH$_2$Cl$_2$ 1:1, 25 °C; (ii) NaBH$_3$CN, MeOH, 25 °C.

## Scheme 6. Synthesis of the Indole Inhibitor 27[a]
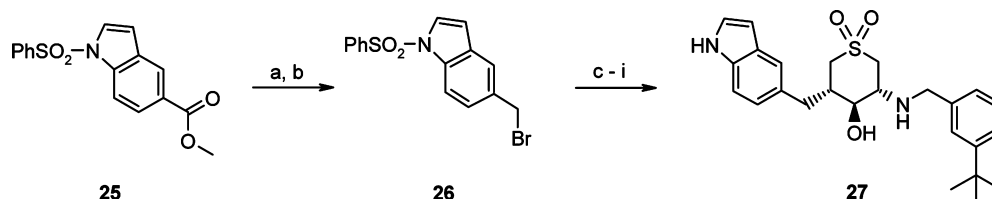


[a]Reagents and conditions: (a) Diisobutylaluminium hydride, THF, 25 °C. (b) CBr$_4$, triphenylphosphine, CH$_2$Cl$_2$, 25 °C. (c) Compound **8**, K$_2$CO$_3$, acetone, 45 °C. (d) (i) Pd(PPh$_3$)$_4$, morpholine, THF, 25 °C; (ii) cat. DBU, THF, 25 °C. (e) LiAlH$_4$, THF, −60 °C. (f) Potassium peroxomonosulfate, THF−H$_2$O 1:1, 25 °C. (g) 5 N HCl in $i$-PrOH, 25 °C. (h) 3-$tert$-Butyl-benzaldehyde, NaOAc, NaBH$_3$CN, MeOH−CH$_2$Cl$_2$ 1:1, 25 °C. (i) 2 N NaOH, MeOH, reflux.

## Scheme 7. Synthesis of the 3-Difluoroethyl-indole Inhibitor 32a[a]



|  |  |  |  |  |
|---|---|---|---|---|
| **28** | **29a** R=CHF$_2$ | **30a** R=CHF$_2$ | **31a** R=CHF$_2$ | **32a** R=CHF$_2$ |
|  | **29b** R=CF$_3$ | **30b** R=CF$_3$ | **31b** R=CF$_3$ | **32b** R=CF$_3$ |
|  | **29c** R=CH$_3$ | **30c** R=CH$_3$ | **31c** R=CH$_3$ | **32c** R=CH$_3$ |

[a]Reagents and conditions: (a) AlCl$_3$, difluoroacetic anhydride, CH$_2$Cl$_2$, 25 °C. (b) Cs$_2$CO$_3$, THF/MeOH 2:1, 25 °C. (c) BH$_3$-THF, THF, 70 °C. (d) NaH, 4-toluenesulfonyl chloride, DMF, 25 °C. (e) Potassium vinyl tetrafluoroborate, bis(triphenylphosphine)palladium(II) dichloride, Cs$_2$CO$_3$, 85 °C. (f) OsO$_4$, $N$-methylmorpholine-$N$-oxide, THF−H$_2$O 2:1, 25 °C. (g) NaBH$_4$, THF−EtOH, 25 °C. (h) PBr$_3$, Et$_2$O, 0−25 °C. (i) (i) Compound **8**, K$_2$CO$_3$, acetone, 25 °C. (j) (i) Pd(PPh$_3$)$_4$, morpholine, THF, 25 °C; (ii) cat. DBU, THF, 25 °C. (k) CaBH$_4$−THF, THF, −78 °C. (l) Potassium peroxomonosulfate, NaOAc, THF−H$_2$O 1:1, 25 °C. (m) 4 N HCl in dioxane, 25 °C. (n) (i) 3-$tert$-Butyl-benzaldehyde, NaOAc, MeOH−CH$_2$Cl$_2$ 1:1, 25 °C; (ii) NaBH$_3$CN, MeOH, 25 °C. (o) 1 N NaOH, MeOH, 50 °C.

prior to metalation with $i$-PrMgCl and trans-metalation with CuI to induce a regioselective (S)-(+)-3,3,3-trifluoro-1,2-epoxypropane ring opening.[50] Removal of the aniline and amino-alcohol protecting groups under standard conditions afforded **48**, whereas O-methylation with NaH and methyl iodide in DMF prior to deprotection gave compound **49**.

## Synthesis of P3 Alkoxy-Substituted Benzyl Sulfone cHEA Inhibitors.

The monosubstituted 3-propyloxy benzyl-substituted cHEA inhibitor **52** (Table 4) was prepared according to Scheme 10. The activated benzyl fragment **51** was synthesized from 1,3-dibromo-5-fluoro-benzene **50**. For possible late stage modifications at C-5, the additional bromine

**Scheme 8. Synthesis of Spiro-Indoline Inhibitor 39a**[a]
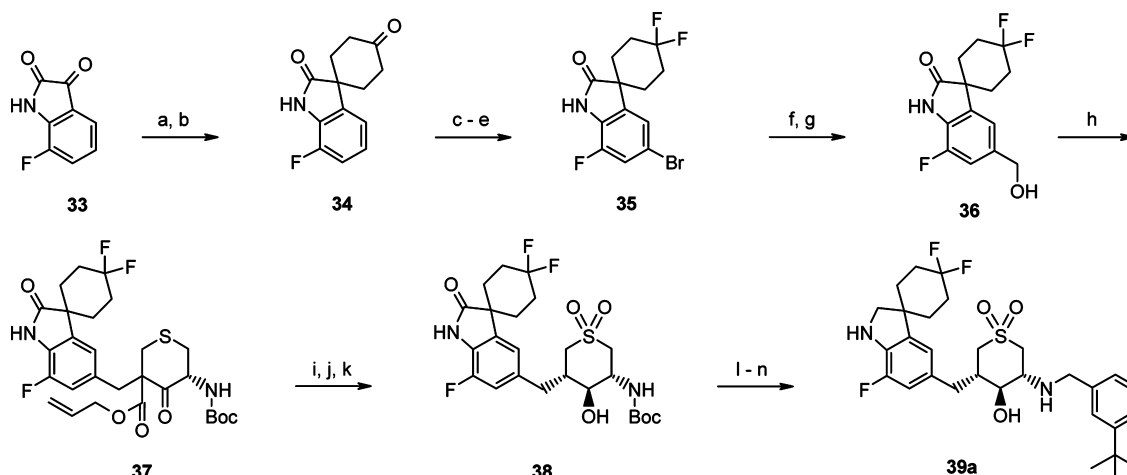


[a]Reagents and conditions: (a) Hydrazine, ethylenglycol, 130 °C. (b) Methyl acrylate, *t*-BuOK, DMSO, 60 °C. (c) H₂NOH−HCl, NaOAc, EtOH, reflux. (d) HF−pyridine, *t*-butylnitrite, CH₂Cl₂, −78 to 25 °C. (e) *N*-Bromosuccinimide, acetonitrile, 25 °C. (f) Potassium vinyl tetrafluoroborate, 1,2,3,4,5-pentaphenyl-1′-(di-*tert*-butylphosphino)ferrocene, triethylamine, *n*-PrOH, reflux. (g) (i) Ozone, NaHCO₃, CH₂Cl₂−MeOH, −78 °C; (ii) NaBH₄, MeOH, 0 °C. (h) Compound **8**, diisopropylazodicarboxylate, triphenylphosphine, THF, 25 °C. (i) (i) Pd(PPh₃)₄, morpholine, THF, 25 °C; (ii) cat. DBU, THF, 25 °C. (j) LiAlH₄, THF, −78 °C. (k) Potassium peroxomonosulfate, NaOAc, THF−H₂O 1:1, 25 °C. (l) 4 N HCl in dioxane, 25 °C. (m) (i) 3-*tert*-Butyl-benzaldehyde, NaOAc, MeOH−CH₂Cl₂ 1:1, 25 °C; (ii) NaBH₃CN, MeOH, 25 °C. (n) LiAlH₄, CHCl₃, THF, 25 °C.

**Scheme 9. Synthesis of P3-Substituted 4-Amino-3-fluoro-aryl cHEA Inhibitors 41, 42, and 44−49**[a]
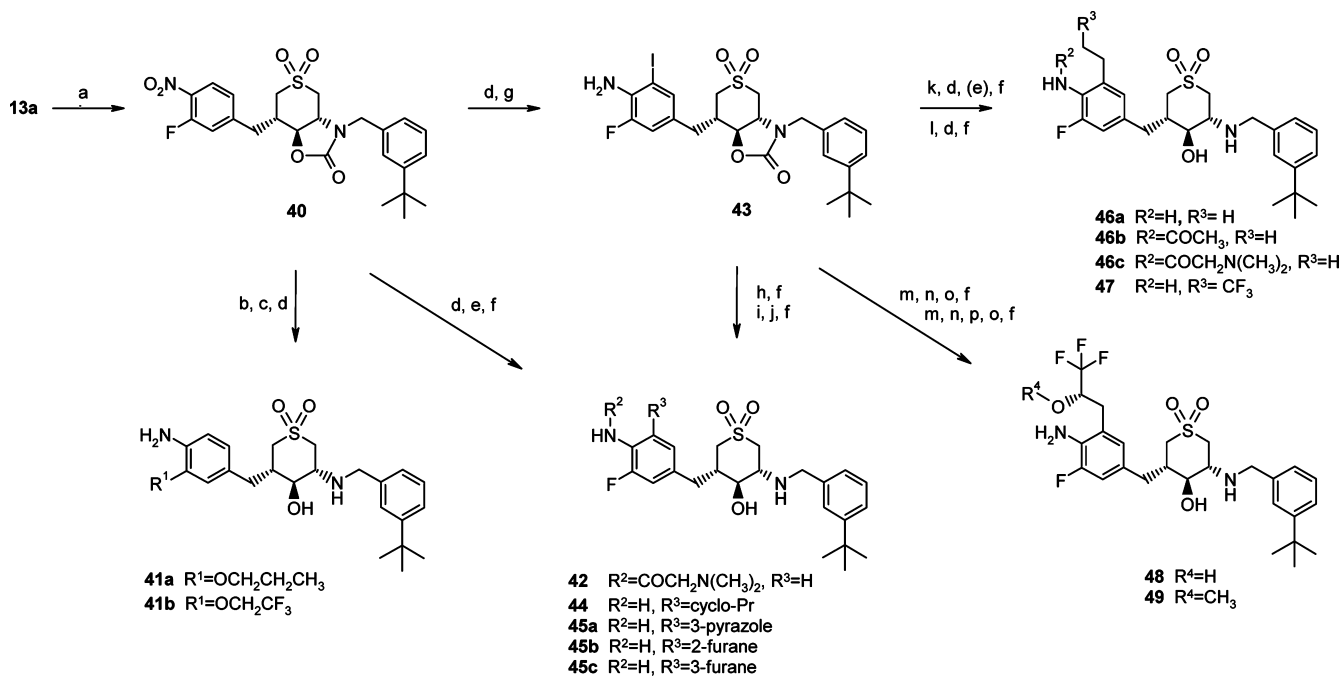


[a]Reagents and conditions: (a) Carbonyldiimidazole, *N,N*-diisopropylethylamine, 4-(*N,N*-dimethylamino)pyridine, acetonitrile, 80 °C. (b) *n*-Propanol, K₂CO₃, DMF, 90 °C. (c) Ba(OH)₂, dioxane−H₂O 2:1, reflux. (d) H₂, 10% Pd−C, THF, 25 °C. (e) *N,N*-Dimethylglycine, propylphosphonic anhydride, *N*-methylmorpholine, DMF, 25 °C. (f) Potassium trimethylsilanolate, THF, 50 °C. (g) Benzyl trimethylammonium-dichloroiodide, CaCO₃, CHCl₃−MeOH 3:1, 60 °C. (h) Cyclopropylboronic acid, bis(triphenylphosphine)palladium(II) dichloride, K₃PO₄, toluene−H₂O 20:1, 105 °C. (i) 2-(Tetrahydro-pyran-2-yl)-2*H*-pyrazole-3-boronic acid, Pd₂(dba)₃, 1,2,3,4,5-pentaphenyl-1-(di-*t*-butylphosphino)-ferrocene, K₃PO₄, dioxane−H₂O, 100 °C. (j) 4 N HCl in dioxane, 25 °C. (k) 2,4,6-Trivinylboroxin−pyridine complex, Pd₂(dba)₃, tri-*tert*-butylphosphine, Cs₂CO₃, dioxane reflux. (l) Trifluoropropyne, *n*-BuLi, ZnCl₂, Pd(PPh₃)₄, THF, −60 °C. (m) Dimethoxymethyl-dimethyl-amine, toluene, microwave, 150 °C. (n) *i*-PrMgCl, CuI, (*S*)-2-trifluoromethyl-oxirane, −25 °C, THF. (o) ZnCl₂, EtOH, 78 °C. (p) NaH, methyliodid, DMF, 25 °C.

substituent was incorporated right from the start and was removed by catalytic hydrogenation for the preparation of **52**.

For an efficient SAR exploration of the S3 pocket with a diverse set of alkoxy fragments linked at C-5 to the 4-amino-3-

fluoro-benzyl P1 fragment, a suitably functionalized, advanced intermediate was required. Preferably, this intermediate should give access to prime side optimization after prior identification of potent P3 fragments with the established 3-*tert*-butyl-benzyl

**Scheme 10. Synthesis of 3-Alkoxy-benzyl-Substituted Sulfone cHEA Inhibitor 52[a]**
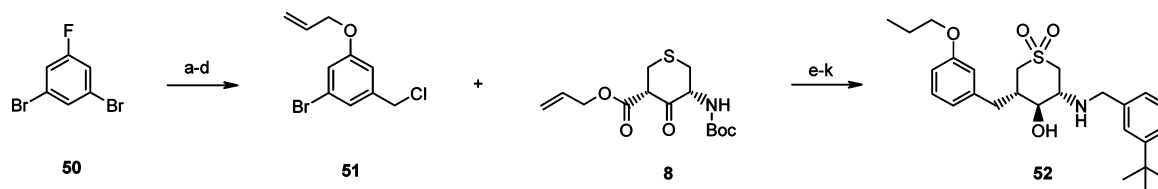


[a]Reagents and conditions: (a) Allylalcohol, t-BuOK, DMSO. (b) (i) n-BuLi, Et$_2$O, −78 °C; (ii) DMF, 5 min. (c) NaBH$_4$, EtOH, 0 °C. (d) Methanesulfonylchloride, N,N-diisopropylethylamine, CH$_2$Cl$_2$, 0 °C to reflux. (e) (i) K$_2$CO$_3$, n-Bu$_4$NI, acetone, reflux; (ii) morpholine, Pd(PPh$_3$)$_4$, THF, 2 h. (f) LiAlH$_4$, THF, −78 °C. (g) Potassium peroxomonosulfate, THF−H$_2$O 1:1, 25 °C. (h) HCl in Et$_2$O, CH$_2$Cl$_2$, 0−25 °C. (i) (i) 3-tert-Butyl benzaldehyde, NaOAc, MeOH−CH$_2$Cl$_2$; (ii) NaCNBH$_3$, 25 °C. (j) H$_2$, Pt−C, THF. (k) H$_2$, Pd−C 10%, EtOH, 25 °C.

**Scheme 11. Synthesis of 3-Alkoxy-substituted 4-Amino-5-fluoro-aryl Inhibitors 60a−q and 62a−i[a]**
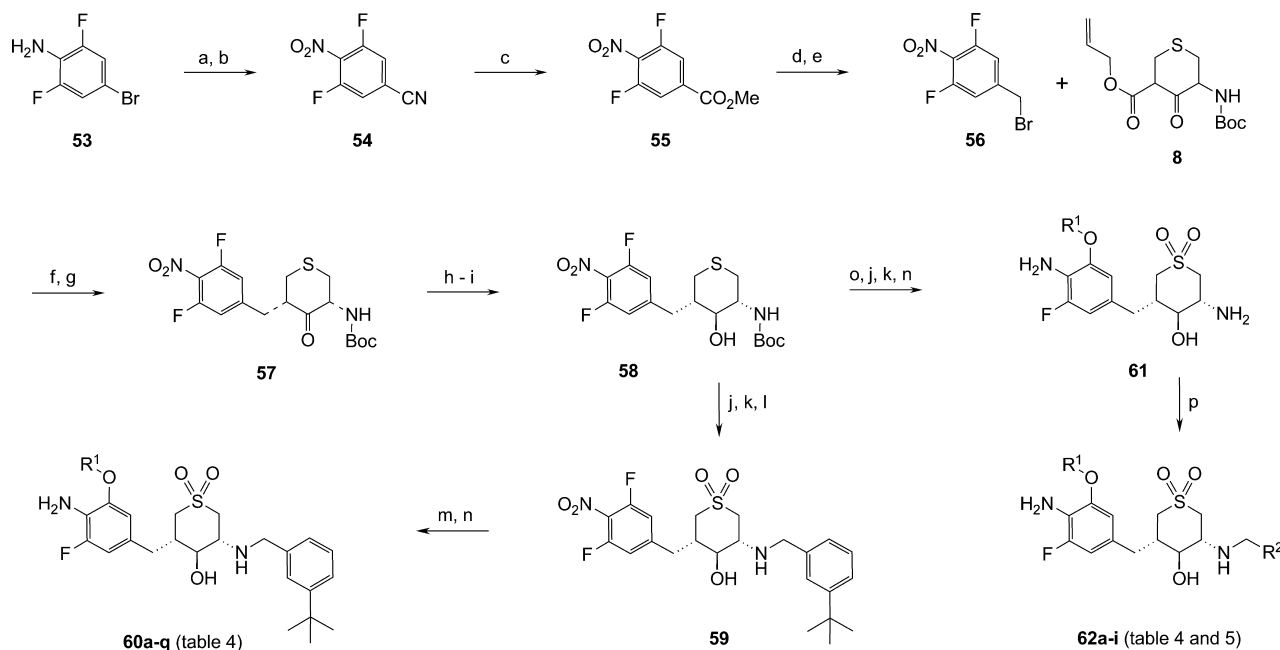


[a]Reagents and conditions: (a) NaBO$_3$ 4H$_2$O, acetic acid, 65 °C. (b) CuCN, N-methylpyrrolidinone, 165 °C. (c) HCl, MeOH, 25−65 °C. (d) Diisobutylaluminium hydride, THF, 0 °C. (e) PBr$_3$, methyl-tert-butylether, 0−25 °C. (f) K$_2$CO$_3$, acetone, 25 °C. (g) (i) Pd(PPh$_3$)$_4$, HCO$_2$H, NEt$_3$, methyl-tert-butylether, 25 °C; (ii) cat. DBU, THF, 25 °C. (h) LiAlH$_4$, THF, −75 °C. (i) Chiralpak AD, heptane−EtOH 3:1. (j) Potassium peroxomonosulfate, THF−H$_2$O 2:1, 25 °C. (k) 4 N HCl in dioxane−THF, 25 °C. (l) (i) 3-tert-Butyl-benzaldehyde, NaOAc; (ii) NaBH$_3$CN, CH$_2$Cl$_2$−MeOH, 25 °C. (m) R$^1$-OH, THF, KOH, 80−100 °C in microwave. (n) NiCl$_2$ 6H$_2$O, NaBH$_4$, MeOH, 0 °C or H$_2$, 10% Pd−C, MeOH−THF 2:1, 45 °C. (o) R$^1$-OH, KHMDS, 0−25 °C, THF. (p) (i) R-CHO, NaOAc; (ii) NaBH$_3$CN, CH$_2$Cl$_2$−MeOH, 25 °C.

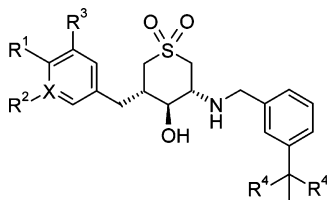P2′ fragment. The N-Boc-protected 3,5-difluoro-4-nitrobenzyl-substituted cHEA scaffold **58** was selected as the central intermediate. The synthesis of this key intermediate is shown in Scheme 11. The commercially available 4-bromo-2,6-difluoro-aniline **53** was oxidized, and the resulting 4-bromo-2,6-difluoro-nitrobenzene was converted into 3,5-difluoro-4-nitrobenzoni-trile **54** with CuCN in N-methylpyrrolidone. Subsequent conversion into 5-(bromomethyl)-1,3-difluoro-2-nitrobenzene was accomplished by standard methodology, methyl-ester formation under Pinner conditions, followed by selective reduction of methyl-ester **55** with diisobutylaluminium hydride to the benzyl alcohol, and subsequent treatment with PBr$_3$ gave the benzyl bromide **56**. The attachment to the keto-ester **8** and the transformation into the central intermediate **58** were carried out by the same reaction sequence as applied previously for the related 3-fluoro-4-nitro-benzyl derivative **11** (Scheme 3). For the initial P3 SAR optimization, **58** was transformed in three steps into the P2′-substituted sulfone cHEA intermediate **59**. S$_N$Ar coupling with various alcohols and subsequent

reduction of the nitro group by catalytic hydrogenation or nickel-borohydride reduction provided the desired inhibitors. For the succeeding P2′ optimization, the S$_N$Ar couplings were carried out with the most potent alkoxide fragments on the N-Boc-protected central intermediate **58**. Potential oxazol-2-one formation was circumvented by use of KHMDS in THF at ambient temperature. Oxidation to the sulfone with potassium peroxomonosulfate, N-Boc deprotection with 4 N HCl in dioxane, and catalytic hydrogenation of the nitro group provided the fully functionalized P3−P1-substituted sulfone cHEA **61**. For the final prime side variation (**62a−i**), the different P2′ fragments were attached in a single step by reductive amination.

## ■ RESULTS AND DISCUSSION

Initial efforts in the 4-hydroxy-benzyl series of cHEA BACE1 inhibitors (**4**, R$^1$=OH, Table 1) revealed that greater passive permeability and decreased P-gp efflux can be achieved as compared to previous acyclic HEA lead compounds (**1**, **2**, and
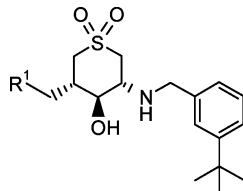
**Table 1. P1 SAR of Benzyl and Heteroaryl-methyl-Substituted Sulfone cHEA Inhibitors**



| compd | $R^1$ | $R^2$ | $R^3$ | $R^4$ | X | IC$_{50}$ ($\mu$M)[a] hBACE1 | hCathD | CHO-APPwt cellular | MDCK $P_{app}$ (nm/s)[b] | ER[c] | brain/blood concn[d] (ratio) |
|---|---|---|---|---|---|---|---|---|---|---|---|
| 4[41] | OH | H | Br | Me | C | 0.055 | 0.44 | 0.76 | 120 | 2 | 0.08/0.05 (1.6) |
| 4a[41] | H | H | H | Me | C | 0.61 | 0.70 | 4.84 | 110 | 1 | |
| 14a | NH$_2$ | F | H | Me | C | 0.35 | 2.52 | 0.63 | 210 | 1 | |
| 14b | NH$_2$ | F | Br | Me | C | 0.055 | 0.34 | 0.45 | 130 | 2 | 0.46/0.20 (2.3) |
| 14c | NH$_2$ | H | Br | Me | C | 0.14 | 0.72 | 0.25 | 130 | 2 | 0.23/0.16 (1.4) |
| 14d | NH$_2$ | F | Br | F | C | 1.37 | 4.16 | 4.98 | 280 | 4 | |
| 14e* | NH$_2$ | H | OCF$_3$ | Me | C | 0.13 | 7.99 | 1.12 | 150 | 2 | 0.29/0.25 (1.2) |
| 15 | NH$_2$ | F | $n$Pr | Me | C | 0.13 | 1.39 | 0.55 | 70 | 2 | 0.33/0.08 (4.1) |
| 18* | NH$_2$ | H | H | Me | N | 1.62 | >10 | 1.36 | 174 | 16 | |

*Racemate. [a]Values are means of at least three experiments. [b]$P_{app}$ is the permeability through a MDR1-MDCK cell monolayer (AP-BL + BL-AP/2). [c]ER is the efflux ratio ($P_{BL-AP}/P_{AP-BL}$) in MDCK cells transfected with human MDR1. [d]Concentrations in brain (nmol/g) and blood (nmol/mL = $\mu$M) obtained 5 min after iv dosage of 0.5 $\mu$mol/kg to mice, using an in vivo cassette screening approach (five compounds dosed together, always including a reference compound to test the reliability of the cassette dosing within a series of similar compounds). Values are means of three animals.

**Table 2. P3−P1 SAR of Bicyclic Heteroaryl-methyl-Substituted Sulfone cHEA Inhibitors**



| compd | $R^1$ | IC$_{50}$ ($\mu$M)[a] hBACE1 | hCatD | CHO-APPwt cellular | MDCK $P_{app}$ (nm/s)[b] | ER[c] | brain/blood concn[d] (ratio) |
|---|---|---|---|---|---|---|---|
| 22* | (indazole) | 1.45 | 3.75 | 1.65 | 230 | 11 | 0.02 / 0.14 (0.1) |
| 24* | (propyl-indazole) | 0.22 | 1.63 | 3.52 | 300 | 49 | 0.02 / 0.20 (1.0) |
| 27* | (indole) | 2.75 | 5.53 | 2.01 | 100 | 3 | 0.23 / 0.17 (1.4) |
| 32a* | $R^2$= CHF$_2$ | 0.055 | 1.22 | 7.42 | 60 | 8 | 0.03 / 0.10 (0.3) |
| 32b* | $R^2$= CF$_3$ | 0.12 | 1.49 | 2.06 | 25 | 7 | 0.05 / 0.24 (0.2) |
| 32c* | $R^2$= CH$_3$ | 0.20 | 2.48 | 0.74 | | | |
| 39a* | (difluorocyclohexyl spiro) | 0.14 | 1.75 | 3.53 | | | |
| 39b* | (cyclobutyl spiro) | 0.56 | 1.72 | 0.08 | 60 | 3 | 0.26 / 0.63 (0.4) |

*Racemate. [a]Values are means of at least three experiments. [b]$P_{app}$ is the permeability through a MDR1-MDCK cell monolayer. [c]ER is the efflux ratio ($P_{BL-AP}/P_{AP-BL}$) in MDCK cells transfected with human MDR1. [d]Concentrations in brain (nmol/g) and blood (nmol/mL = $\mu$M) obtained 5 min after iv dosage of 0.5 $\mu$mol/kg to mice, using an in vivo cassette screening approach (five compounds dosed together, always including a reference compound to test the reliability of the cassette dosing within a series of similar compounds).

3, Figure 2).[41] The improved physicochemical properties of 4 resulted in a good brain/blood concentration ratio (about 2) and a moderate brain concentration (0.08 nmol/g) in mice at 5 min after intravenous injection of 0.5 $\mu$mol/kg (in vivo cassette screening approach). Encouraged by this result, we continued to further optimize the potency, selectivity, and metabolic stability by substitution of the 4-hydroxy-benzyl P1 residue with more stable P1 and P3 groups, the latter via P1-extended

moieties. To retain the binding contribution of the H-bond[41] of the 4-hydroxy-benzyl substituent to the C=O of Phe108 (Figure 4), we searched for alternative substituted benzyl and bicyclic heteroaryl-methyl ring systems (Tables 1 and 2) containing a HBD with greater metabolic stability.

**P1 SAR of Benzyl and Heteroaryl-methyl-Substituted Sulfone cHEA Inhibitors.** The *ortho*-halogenated anilines **14a−c**, which were predicted[51] and confirmed to be non-mutagenic and nongenotoxic in the AMES and micronucleous assay, exhibited moderate potency ($IC_{50}$ = 55−350 nM), with minimal P-gp-mediated efflux (ER = 1−2). To further increase the selectivity of compounds **4** and **14a−c** against CatD (5−10-fold), the amino-pyridine analogue **18** was prepared, as it contains a stronger HBD functionality for the H-bonding interaction to Phe108. Because this modification lowered the potency and induced a strong P-gp-mediated efflux (ER = 16), no further extensions into the S3 pocket were explored for this series. On the other hand, the good cellular activity of **14c** (Table 1, $IC_{50}$ 250 nM) and the promising *in vivo* brain/blood concentration ratios of **14b, c, e** and **15** (Table 1) encouraged us to improve potency and selectivity of P3 extensions linked to benzyl and bicyclic heteroaryl-methyl P1 residues. The cocrystal structure of **14d** in BACE1 (Figure 6) bearing a
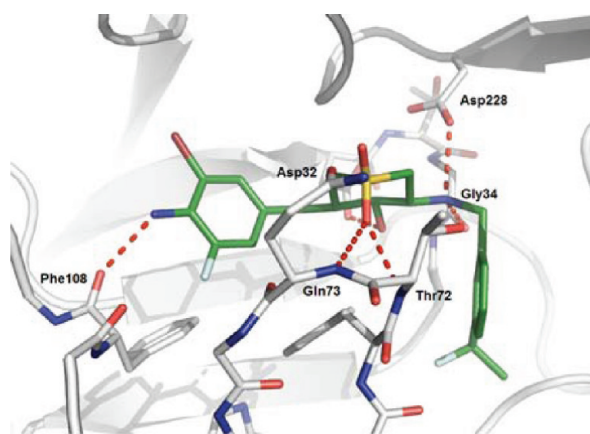


**Figure 6.** Cocrystal structure of **14d** (green) in BACE1 (gray).

*meta*-CF₂CH₃ group instead of a C(CH₃)₃ in the P2′ position confirmed that the designed binding interactions were fully formed, including H-bonding with Asp32, Asp228, and Gly34, as well as with the backbone amides of Phe108 and of the flap residues Thr72 and Gln73. Compound **14d** binds to a closed conformation of the flap, similar to the acyclic HEA inhibitor **3**.

In addition, excellent hydrophobic contacts were observed in the adjacent P1 and P2′ subpockets, explaining the promising submicro molar enzymatic activity of **14b** ($IC_{50}$ = 55 nM). Further extensions into the barely filled S3 pocket (Figure 7) should indeed lead to a further increase in potency and selectivity.

**P3−P1 SAR of Bicyclic Heteroaryl-methyl-Substituted Sulfone cHEA Inhibitors.** Molecular modeling suggested that the P1 pocket can be fully occupied equally well with an indazole, indole, and indoline residue as compared to aniline **14b**. The BACE1 inhibition data of the indazole **22** and indole **27** and corresponding P3 extended inhibitors **24**, **32a−c**, and **39a,b** (Table 2) show that the 3-(2,2-difluoro-ethyl)-substituted indole **32a** is the most potent compound in this series ($IC_{50}$ = 55 nM). The 50-fold potency increase over the C-3 unsubstituted analogue **27** indicated a substantial binding
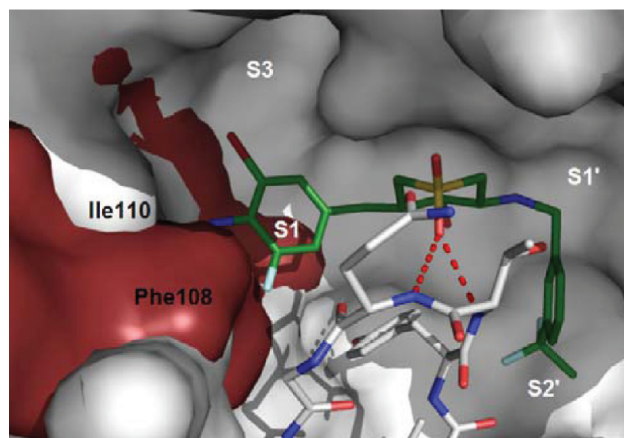


**Figure 7.** Cocrystal structure of **14d** (green) in BACE1 (gray surface) and an overlay of the CatD surface (ruby; PDB code: 1lyb).

contribution by the rather small 3-(2,2-difluoro-ethyl) P3 substituent. A similar gain in potency could not be observed with the *n*-propyl extension on the less potent indazole analogues **24** or aniline **15** (Table 1) and ethyl extension on indole **32c**. In addition, the indazole analogues seemed to be good P-gp substrates according to the high ER in the MDR1-MDCK assay, probably because of the additional HBA. Disappointingly, the 4,4-difluorospiro[cyclohexane-1,3′-indolin] analogue **39a**, designed to maximize the hydrophobic contacts in the S3 pocket, was 3-fold less active than the 3-(2,2-difluoro-ethyl)-substituted indole **32a**. To better understand the preliminary P3 SAR for the design of more potent P3 fragments, cocrystal structures of **32a** (Figure 8A) and **39a**
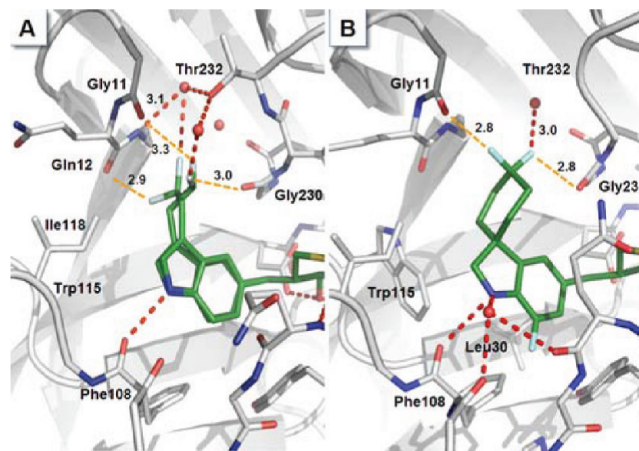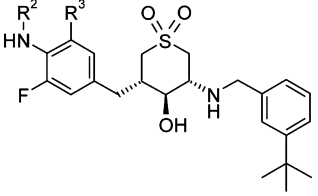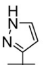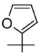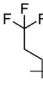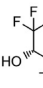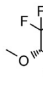


**Figure 8.** (A) Cocrystal structure of **32a** (green) in BACE1 (gray), showing two alternate conformations for the P1−P3 group. (B) Cocrystal structure of **39a** (green) in BACE1 (gray). Distances are reported in Å.

(Figure 8B) with BACE1 were obtained. In both structures, hydrophobic interactions to Leu30, Trp115, and Ile118, as well as different types of favorable nonbonding protein−fluorine interactions,[52] could be confirmed. Beside short orthogonal C−F contacts to the amide C=O of Gly11 and Gly230, additional hydrogen bonds to the side chain of Thr232 and to a deeply buried water (2.8−3.3 Å) were observed in the complex with **32a** as well as with **39a**. Interestingly, two alternate conformations were observed for the 3-(2,2-difluoro-ethyl)-indole group of **32a**. In one conformation, similar C−F

**Table 3. P3 SAR of 4-Amino-3-fluoro-benzyl Substituted P3−P1 Sulfone cHEA Inhibitors**



| | | | IC$_{50}$ ($\mu$M)[a] | | | | | |
|---|---|---|---|---|---|---|---|---|
| compd | R$^2$ | R$^3$ | hBACE1 | hCatD | CHO-APPwt cellular | MDCK $P_{app}$ (nm/s)[b] | ER[c] | clogP[d] |
| 14a | H | H | 0.35 | 2.52 | 0.63 | 210 | 1 | 2.2 |
| 42 | (CH$_3$)$_2$NCH$_2$CO | H | 0.061 | >10 | 0.30 | 60 | 19 | 2.3 |
| 46a | H | CH$_3$CH$_2$ | 0.87 | 2.0 | 1.77 | 230 | 2 | 3.5 |
| 46b | CH$_3$CO | CH$_3$CH$_2$ | 0.008 | 2.3 | 0.56 | 170 | 41 | 2.4 |
| 46c | (CH$_3$)$_2$NCH$_2$CO | CH$_3$CH$_2$ | 0.052 | >10 | 0.04 | 130 | 77 | 2.4 |
| 15 | H | CH$_3$CH$_2$CH$_2$ | 0.13 | 1.39 | 0.66 | 70 | 1 | 4.0 |
| 44 | H | (isopropyl) | 0.094 | 1.74 | 0.58 | 160 | 3 | 3.2 |
| 45a* | H | (pyrazolyl) | 0.028 | 0.60 | 0.35 | 200 | 17 | 2.8 |
| 45b | H | (furanyl) | 0.079 | 0.36 | 1.38 | 20 | 2 | 3.8 |
| 45c | H | (furanyl) | 0.15 | 0.51 | 2.35 | 30 | 2 | 3.6 |
| 47 | H | (CF$_3$ alkyl) | 0.13 | 0.98 | 0.37 | 110 | 3 | 3.4 |
| 48 | H | (CF$_3$ hydroxy alkyl) | 0.049 | 1.05 | 0.24 | 130 | 20 | 2.2 |
| 49 | H | (CF$_3$ methoxy alkyl) | 0.078 | 1.14 | 0.41 | 90 | 4 | 3.0 |

*Racemate. [a]Values are means of at least three experiments. [b]$P_{app}$ is the permeability through a MDR1-MDCK cell monolayer. [c]ER is the efflux ratio ($P_{BL-AP}/P_{AP-BL}$) in MDCK cells transfected with human MDR1. [d]clog $P$ values are calculated by BioByte.

contacts as described above for **39a** were found, while an additional short orthogonal C−F contact to the C=O of Gln12 was observed for the second conformation. The 4,4-difluorospiro[cyclohexane-1,3′-indolin]-substituted inhibitor **39a** was individually designed to gain further potency and selectivity by maximizing the hydrophobic contacts in the S3 pocket. The minor 4-fold increase in potency against the smaller spiro-cyclobutyl analogue **39b** can be explained by an energetically unfavorable enlargement of the S3 pocket as observed in the cocrystal structure of **39a**. The α-CH$_2$ of the spiro-cyclohexyl and the sp3-hybridized carbon at C2 of the indoline ring are close to the hydrophobic wall formed by Leu30, Trp115, and Ile118. This is not the case in the more potent indole analogue **32a**, where the now sp2-hybridized carbon can form a favorable C−H⋯π interaction with Trp115. The positive effect of a fully occupied S3 pocket on the selectivity over CatD could be demonstrated by comparison of the spiro-cyclohexyl- and spiro-cyclobutyl-substituted compounds (CatD IC$_{50}$ = 3530 vs 80 nM, respectively). An overall assessment of the in vitro profile of the bicyclic heteroaryl-methyl versus the benzyl-substituted cHEA inhibitors indicated that the monocyclic P1 residues tend to have a better cellular

activity, higher permeability and brain/blood ratio, and a lower P-gp efflux.

**P3−P1 SAR of Substituted Benzyl Sulfone cHEA Inhibitors.** The N-acylation of the aniline in combination with an ethyl substituent in the *ortho*-position resulted in the highly potent inhibitors **46b** and **46c** with excellent selectivity (>100-fold) and good cellular activity (**46c**, IC$_{50}$ = 40 nM), good permeability, but very high P-gp efflux (ER = 41−77). The additional HBA is most likely responsible for this detrimental effect since the nonacylated analogue **46a** has a very low ER of 2. Modeling predicted some gain in potency by filling S3 with cyclic moieties; this prediction was confirmed with examples **44** and **45b−c** (Table 3). The analysis of the cocrystal structure of **14d** (Figure 6) suggested that additional potency could be gained by optimizing potential H-bonds to proximal residues and deeply buried water molecules at the surface of the S3 pocket. This could be confirmed by examples **45a** (IC$_{50}$ = 28 nM) and **48** (IC$_{50}$ = 49 nM). Unfortunately, the newly introduced HBD moieties contributing to improved potency were equally well recognized by P-gp, resulting in high P-gp-mediated efflux, as illustrated by **45b,c** and **47** versus **45a** and **48** (ER = 2−3 → 17−20). Only the CF$_3$ group, making

weak nonbonding protein−fluorine interactions, as well as the methyl-ether functionality, a weak HBA, were barely influencing P-gp recognition (**49**, $IC_{50}$ = 78 nM, ER = 4). The overall binding motif determined in the cocrystal structure of **48** with BACE1 (Figure 9A) is quite similar to the bicyclic P3−P1
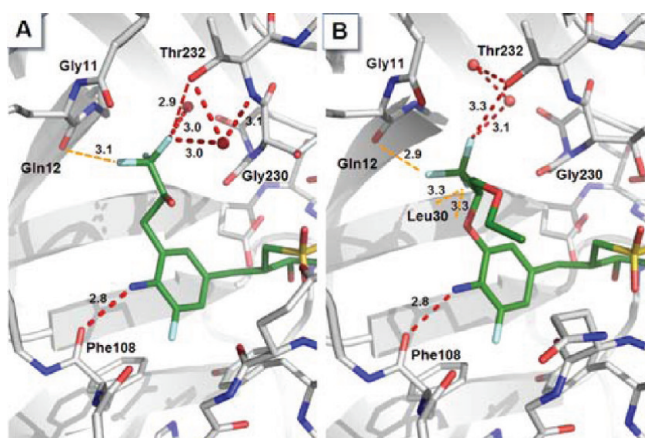


**Figure 9.** (A) Cocrystal structure of **48** (green) in BACE1 (gray). (B) Cocrystal structure of **60n** (green) in BACE1 (gray). Distances are reported in Å.

inhibitors **32b** and **39a** (Figure 8). The beneficial interactions like the short orthogonal C−F contact to the amide C=O of Gln12 (3.1 Å) and the H-bonding to the OH of Thr232 (2.9 Å) and to the deeply buried water (3.0 Å) were observed again. The high lipophilicity of **15** and **45b,c** (clog $P$ > 3.5) and lower conformational flexibility of carbon versus potentially oxygen-linked P3 fragments had an overall negative impact on permeability. Therefore, the more polar alkoxy P3 extensions were explored (Table 4).

A comparison of enzymatic potency, cell activity, and selectivity of the initial P3 alkoxy-substituted 4-amino-fluoro-benzyl cHEA inhibitors with the isosteric P3 alkyl analogues (i.e., **60b** versus **15** in Table 4) demonstrated a >5-fold improvement in these parameters. The major contribution of the 4-amino group to potency, selectivity, and permeability becomes evident by comparison of **41a** with **52** ($IC_{50}$ = 45 nM, >100-fold selectivity, $P_{app}$ = 70 nm/s vs $IC_{50}$ = 670 nM, no selectivity, $P_{app}$ = 20 nm/s). In an attempt to further improve the in vitro activity of this promising lead, a small library of different alkoxy- and fluorine-substituted P3-alkoxy fragments (Table 4), primed to optimally occupy the S3 pocket, was generated and attached at C-5 to the 4-amino-3-fluoro-benzyl P1 residue. The further optimization of the P3-alkoxy fragments, especially the nonbonding protein−fluorine interactions, was very rewarding in terms of further potency and selectivity enhancement (**60b** vs **60j**, **60n**, **60p**, $IC_{50}$ = 24 nM → 2 nM, selectivity 50- → >100-fold). Analysis of the cocrystal structure of **60n** in BACE1 (Figure 9B) confirmed that the more flexible alkoxy P3 extensions could more efficiently form the individual protein−fluorine interactions as compared to the conformationally more rigid alkyl isosters and that the distal ethoxy moiety does not contribute to binding, as indicated by the SAR (**60m**, **60n**, **60p**, and **60q** are equipotent in vitro). The excellent orthogonal C−F contact to the amide C=O of Gln12 (2.9 Å), the nonpolar hydrogen contacts to both methyl groups of Leu30 (3.3 Å) and H-bonds to a deeply buried water (3.1 Å), and the OH of Thr232 (3.3 Å) reveal that a nearly perfect
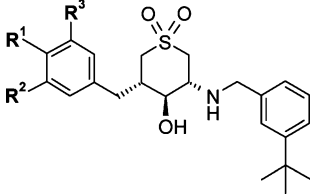
P3 fragment has been identified. The additional polarity enhancing alkoxy moiety in **60n−q** forms an additional H-bond to the structured water molecules between the flap (Gln73) and the residues at the back of the cavity.
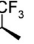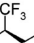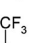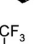
As predicted from the slightly smaller CatD S3 pocket (Figure 7), the selectivity against this enzyme could be considerably improved with larger P3 fragments. The 40-fold selectivity of the initial lead (**60b**) containing a small P3-ethoxy fragment was increased to >100-fold with a difluoro-ethoxy (**60g**) and to 450-fold with the bulky hexafluoroisopropoxy fragment of the potent inhibitor **60j** (enzymatic $IC_{50}$ = 2 nM). On the other hand, despite extensive P3 modifications, only a 2−3-fold improvement in the cellular activity was achieved (**60g**, $IC_{50}$ = 72 nM; **60p**, $IC_{50}$ = 55 nM) over the initial lead compound **60b** ($IC_{50}$ = 150 nM). The rather low basicity of the sulfone cHEA type inhibitors ($pK_a$ = 5.4−5.8) is most likely responsible for the large shift between the enzymatic and the cellular activity, since good cell permeation can be assumed for all compounds, based on the moderate-to-high permeability in the MDR1-MDCK permeability assay.

In vitro metabolite identification studies with **60b** using mouse and human liver microsomes indicated the formation of the phenolic metabolite **60e**. Substitution of the small P3-ethoxy fragment by more stable ethers (**60c**, **60d**) and fluorinated alkylethers (**60f−j**) increased the metabolic stability but also the clog $P$. With the bulky hexafluoroisopropyl fragment (**60j**), the formation of this undesired metabolite **60e** was completely abolished. In an attempt to improve the low permeability ($P_{app}$ = 30 nm/s) caused by the lipophilic hexafluoroisopropoxy fragment (clog $P$ = 4.2 for **60j**), one of its $CF_3$ groups was substituted by an alkyl-ether moiety (**60m−q**), to reduce lipophilicity and to increase solubility. Previously established SAR indicated that distal methyl-ether containing P3 fragments did retain good cellular activity and permeability (**60k**, $P_{app}$ = 250 nm/s), and triggered only a minor increase in P-gp-mediated efflux (**49** and **60k**). Gratifyingly, the further optimization of the P3 fragment led to the identification of the (*R*)-1-methoxymethyl-2,2,2-trifluoro-ethoxy substituted inhibitor **60p**, a highly potent and selective analogue of **60j** ($IC_{50}$ = 2 nM, selectivity > 100-fold) with equal cellular activity ($IC_{50}$ = 50 nM) and an improved profile (reduced clog $P$ = 4.2 → 3.5, increased $P_{app}$ = 30 → 130 nm/s, retained ER = 4 → 5).

**P2′ SAR of Sulfone cHEA Inhibitors.** The pharmacokinetics of the nonprime side optimized cHEA inhibitors (Table 6) indicated high metabolism. In vitro metabolite identification studies with **60h** and **60j** using liver microsomes suggested that *N*-benzylic oxidation was the main site of metabolism as observed in other HEA inhibitors.[38j] However, our sulfone cHEA inhibitors strongly depended on *N*-benzyl-linked P2′ fragments for potency (**62a**, **62b** vs **60j**), and steric interference with the cHEA scaffold prohibited the removal of the metabolic soft spot by substitution. We consequently focused our attempts at improving metabolic stability on reducing lipophilicity (clog $P$). As shown in Table 5 with representative examples, the incorporation of polar functionalities or more polar heterocyclic ring systems led in most cases to a strong increase in P-gp-mediated efflux. A partial exception was the 3-trifluoromethoxy-benzyl analogue **62g** ($IC_{50}$ = 44 nM, ER = 6, clog $P$ = 3.4). The reduced lipophilicity (clog $P$ 4.2 → 3.4) showed a beneficial effect on the inhibition of CYP3A4 inhibition ($IC_{50}$ = 0.3 → 9.2 $\mu$M) as compared to **60j**. Unfortunately, the improved profile of **62g** did not have an impact on the large shift between the enzymatic and the cellular

**Table 4. P3 SAR of 3-Alkoxy-Substituted Benzyl Sulfone cHEA Inhibitors**



| compd | $R^1$ | $R^2$ | $R^3$ | IC$_{50}$ ($\mu$M)[a] hBACE1 | hCatD | CHO-APPwt cellular | MDCK $P_{app}$ (nm/s)[b] | ER[c] | clogP[d] |
|---|---|---|---|---|---|---|---|---|---|
| 15 | NH$_2$ | F | CH$_2$CH$_2$CH$_3$ | 0.130 | 1.39 | 0.660 | 70 | 1 | 4.0 |
| 52 | H | H | OCH$_2$CH$_2$CH$_3$ | 0.670 | 0.29 | 4.450 | 20 | 1 | 4.4 |
| 41a | NH$_2$ | H | OCH$_2$CH$_2$CH$_3$ | 0.045 | 5.20 | 0.115 | 70 | 2 | 3.5 |
| 41b | NH$_2$ | H | OCH$_2$CF$_3$ | 0.036 | 4.37 | 0.310 | 230 | 3 | 3.2 |
| 60a | NH$_2$ | F | OCH$_2$CH$_2$CH$_3$ | 0.056 | 2.22 | 0.424 | 70 | 3 | 3.8 |
| 60b | NH$_2$ | F | OCH$_2$CH$_3$ | 0.024 | 1.03 | 0.150 | 180 | 3 | 3.3 |
| 60c | NH$_2$ | F | O–◇ | 0.011 | 0.39 | 0.215 | 60 | 3 | 3.6 |
| 60d | NH$_2$ | F | O–◻–O | 0.025 | 1.15 | 0.118 | 230 | 24 | 2.3 |
| 60e | NH$_2$ | F | OH | 0.120 | 0.54 | 1.413 | 140 | 27 | 2.3 |
| 60f | NH$_2$ | F | OCH$_2$CH$_2$F | 0.043 | 2.00 | 0.225 | 260 | 16 | 3.7 |
| 60g | NH$_2$ | F | OCH$_2$CHF$_2$ | 0.006 | 0.68 | 0.072 | 220 | 10 | 3.3 |
| 60h | NH$_2$ | F | OCH$_2$CF$_3$ | 0.006 | 0.69 | 0.116 | 250 | 5 | 3.5 |
| 60i | NH$_2$ | F | OCH$_2$CH$_2$CF$_3$ | 0.075 | 2.40 | 1.03 | 120 | 4 | 3.5 |
| 60j | NH$_2$ | F | OCH(CF$_3$)$_2$ | 0.002 | 0.90 | 0.055 | 30 | 4 | 4.2 |
| 60k | NH$_2$ | F | OCH$_2$CH$_2$OCH$_3$ | 0.100 | 3.98 | 0.382 | 250 | 8 | 2.6 |
| 60l | NH$_2$ | F | O–CH(CH$_3$)$_2$ | 0.043 | 2.22 | 0.443 | 140 | 3 | 3.6 |
| 60m | NH$_2$ | F | O–CH(CF$_3$)CH$_3$ | 0.003 | 0.48 | 0.105 | 100 | 5 | 3.8 |
| 60n | NH$_2$ | F | O–CH(CF$_3$)CH$_2$O-Et | 0.002 | 0.23 | 0.126 | 110 | 2 | 3.9 |
| 60o | NH$_2$ | F | O–CH(CF$_3$)CH$_2$O-Et | 0.032 | 1.23 | 0.346 | 80 | 2 | 3.9 |
| 60p | NH$_2$ | F | O–CH(CF$_3$)CH$_2$O-Me | 0.002 | 0.25 | 0.050 | 130 | 5 | 3.5 |
| 60q | NH$_2$ | F | O–CH(CF$_3$)CH$_2$O-CH$_2$CH$_2$O-Me | 0.004 | 0.25 | 0.131 | 120 | 4 | 3.4 |

[*]Racemate. [a]Values are means of at least three experiments. [b]$P_{app}$ is the permeability through a MDR1-MDCK cell monolayer. [c]ER is the efflux ratio ($P_{BL-AP}/P_{AP-BL}$) in MDCK cells transfected with human MDR1. [d]clog $P$ values are calculated by BioByte.
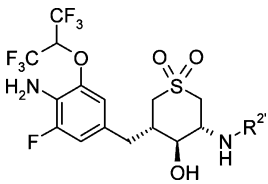
activity (IC$_{50}$ = 44 vs 950 nM, respectively). In comparison to the initial 3-*tert*-butyl-benzyl P2′ residue of **60j**, no equipotent prime side fragment with improved metabolic stability and adequate permeability properties could be identified.
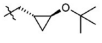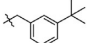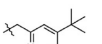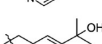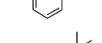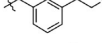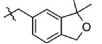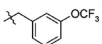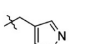
**In Vivo Pharmacokinetics.** The pharmacokinetic parameters of selected cHEA inhibitors were investigated in mice (Table 6). In general, compounds from this series displayed high systemic blood clearance. The only exception was the initial lead compound **14c**, which displayed low blood clearance (8 mL/min/kg) but had a poor oral bioavailability (possibly due to its poor solubility). After 30 and 60 $\mu$mol/kg, substantial blood and brain levels were observed (3−4 $\mu$M in blood and ∼2 nmol/g in brain after 1 h postdose), and a moderate brain penetration (brain/blood concentration ratios of 0.5 and 0.6, respectively) was derived. In vitro studies indicated that **60h** and **60j** are extensively oxidized by CYP3A4 enzyme, which was illustrated in vivo by a high total blood clearance of 111 and 82 mL/min/kg, respectively, that is, near the hepatic blood flow in mice (90 mL/min/kg).[53] The nonlinear pharmacokinetic profile (as indicated by the substantial overproportional

increase of the AUC values between 6 and 60 $\mu$mol/kg oral dose) suggested strong saturation of metabolism at the high oral dose. The challenge remained to find inhibitors that combine the reasonable PK profile of the initial lead **14c**, with the good potency/selectivity of **60h** and **60p**.

**Reduction of A$\beta$ in APP51/16 Transgenic Mice.** To assess the effect of BACE1 inhibition on brain levels of A$\beta_{40}$, selected compounds with good cellular activity (IC$_{50}$ < 150 nM) and a moderate-to-low P-gP efflux (ER ≤ 5) were tested in human wild-type APP transgenic mice (APP51/16). After oral administration of 180 $\mu$mol/kg, exposure in blood and brain, as well as A$\beta_{40}$ and C99 forebrain concentrations were measured at 4 h postdose. The results of these experiments are shown in Table 7. They show a maximal reduction of A$\beta_{40}$ of 31−34% ($p$ < 0.001 vs vehicle-treated group, two-tailed Student's $t$ test) for inhibitors **60b**, **60h**, and **60p**. Usually, a slightly higher reduction of the C-terminal fragment C99 was observed (34−54%, $p$ ≤ 0.05). Inhibitor **60g**, possessing an increased P-gP-ER (ER 10), showed, as expected, a lower A$\beta_{40}$ reduction, despite high blood exposure. The low efficacy of the

**Table 5. P2′ SAR of 4-Amino-3-fluoro-5-hexafluoroisopropoxy-benzyl Sulfone cHEA Inhibitors**



| compd | R$^1$ | IC$_{50}$ ($\mu$M)$^a$ hBACE1 | hCatD | CHO-APPwt cellular | MDCK $P_{app}$ (nm/s)$^b$ | ER$^c$ | clogP$^d$ | IC$_{50}$ ($\mu$M)$^a$ CYP3A4 |
|---|---|---|---|---|---|---|---|---|
| 62a | H | >10 | >10 | . | 130 | 17 | 0.1 | |
| 62b | | >10 | 3.71 | | | | 2.3 | |
| 60j | | 0.002 | 0.45 | 0.055 | 30 | 4 | 4.2 | 0.3 |
| 62c | | 0.068 | 3.07 | 0.37 | 380 | 17 | 2.7 | 0.4 |
| 62d | | 0.002 | 1.32 | 0.17 | 110 | 30 | 2.0 | 2.1 |
| 62e | | 0.002 | 0.60 | 0.21 | 120 | 35 | 2.4 | 0.8 |
| 62f | | 0.006 | 1.51 | 0.13 | 210 | 15 | 2.9 | 0.7 |
| 62g | | 0.044 | 2.53 | 0.95 | 120 | 6 | 3.4 | 9.2 |
| 62h | | 0.036 | 2.81 | 0.38 | 160 | 46 | 2.3 | 6.7 |
| 62i | | 0.007 | 0.51 | 0.47 | 200 | 8 | 2.5 | 0.4 |

$^a$Values are means of at least three experiments. $^b P_{app}$ is the permeability through a MDR1-MDCK cell monolayer. $^c$ER is the efflux ratio ($P_{BL-AP}/P_{AP-BL}$) in MDCK cells transfected with human MDR1. $^d$clog $P$ values are calculated by BioByte.

**Table 6. Pharmacokinetic Properties of P1-Substituted Benzyl Sulfone cHEA Inhibitors**

| compd | dose ($\mu$mol/kg) | AUC$_{inf}$ (pmol h/mL) | blood CL (mL/min/kg) | Vdss (L/kg) | $t_{1/2}$ (h) | $F^d$ (%) | brain/blood concn (ratio) (nmol/g)/(nmol/mL)$^f$ 1 h pd$^e$ | 4 h pd$^e$ |
|---|---|---|---|---|---|---|---|---|
| 14c | 2 iv$^a$ | 4093 | 8.1 | 1.6 | 4.0 | | | |
| | 30 po$^b$ | 6432 | | | | 10 | | |
| | 60 po$^b$ | | | | | | 2.17/4.07 (0.5) | 1.92/2.98 (0.6) |
| 60h | 2 iv$^a$ | 300 | 111 | 7.2 | 1.4 | | 0.11/0.06 (1.8) | 0.01/0.01 (1.0) |
| | 6 po$^b$ | 466 | | | | 52 | 0.08/0.03 (2.7) | 0.11/0.01 (11) |
| | 60 po$^b$ | 14837 | | | | | 1.19/4.10 (0.3) | 0.55/1.86 (0.3) |
| 60j | 2 iv$^a$ | 407 | 82 | 16.3 | 2.9 | | | |
| | 6 po$^c$ | 398 | | | | 32 | 0.02/0.06 (0.3) | 0.01/0.03 (0.3) |
| | 60 po$^c$ | 4071 | | | | 33 | 0.23/0.47 (0.5) | 0.15/0.19 (0.8) |

$^a$The vehicle for mouse iv dosing was N-methyl pyrrolidone/blank plasma (10:90 v/v). $^b$The vehicle for mouse po dosing was carboxymethylcellulose 0.5% w/v in water/Tween 80 (99.5/0.5, v/v). $^c$The vehicle for mouse po dosing was solutol HS15/propylenglycol/citrate buffer, pH 4.75, 50 mM (10/5/85, v/v/v). $^d$The oral bioavailability was calculated by dividing the dose-normalized oral and intravenous AUC values, assuming a linear pharmacokinetics between the dose regimens. $^e$pd, postdose. $^f$Mean of brain and blood concentrations ($n = 3$) measured by LC/MS/MS.

highly potent inhibitor **60j** can be explained by the low cellular permeability and high lipophilicity, leading to a potential increase of nonspecific binding in the brain compartment.

## ■ CONCLUSION

Over the past decade, the challenges associated with BACE1 inhibitor design proved to be substantial. Despite the experience gained in the field of HIV and renin inhibitors, it remains difficult to find highly potent and selective, low molecular weight inhibitors demonstrating good pharmacokinetic and BBB penetration properties. By structure- and property-based design, a cyclic HEA TS mimetic that allowed direct tethering of the P3 to the P1 residue was invented. This new, nonpeptidic scaffold allowed the reduction of MW and HBA functionalities, leading to inhibitors with good BBB penetration properties. Optimization of potency and selectivity

**Table 7. PK-PD of 3-Alkoxy-Substituted Benzyl Sulfone cHEA Inhibitors**

| compd | CHO-APPwt cells IC$_{50}$ ($\mu$M) | $P_{app}$[a] (nm/s) | ER[b] | brain/blood concn[c] | 4 h pd[d] (%)[e] | |
| --- | --- | --- | --- | --- | --- | --- |
| | | | | | brain A$\beta$40 reduction | brain C99 reduction |
| **60b** | 0.15 | 180 | 3 | 3.1/9.0 | 34 ($p < 0.001$) | 54 ($p = 0.004$) |
| **60g** | 0.07 | 220 | 10 | 2.1/12.2 | 18 ($p < 0.001$) | 32 ($p = 0.02$) |
| **60h** | 0.12 | 250 | 6 | 1.8/10.2 | 31 ($p < 0.001$) | 34 ($p = 0.06$) |
| **60j** | 0.08 | 30 | 4 | 1.5/3.7 | 6 ($p = 0.4$) | 22 ($p = 0.16$) |
| **60p** | 0.05 | 130 | 5 | 1.9/7.3 | 31 ($p < 0.001$) | 48 ($p < 0.001$) |

[a]$P_{app}$ is the passive permeability through a MDR1-MDCK cell monolayer. [b]ER in MDCK cells ($P_{BL-AP}/P_{AP-BL}$) transfected with human MDR1. [c]Concentrations in brain (nmol/g) and blood (nmol/mL = $\mu$M) obtained at 4 h after po dosage of 180 $\mu$mol/kg to APP51 transgenic mice. The oral formulation was a suspension in water containing 0.25 or 0.5% methylcellulose. [d]pd, postdose. [e]% mean reduction as compared to the mean of the vehicle control.

provided **60h** and **60p**, two selective, low nanomolar BACE1 inhibitors effective in reducing A$\beta$ levels in APP51/16 mice. The moderate cellular activity and the poor pharmacokinetic profile remain to be resolved. Efforts to address these liabilities will be the subject of future communications.

## ■ EXPERIMENTAL SECTION

**General.** All reagents were obtained from commercial suppliers and used without further purification unless noted otherwise. Anhydrous solvents were obtained from Aldrich and used directly. All reactions involving air- or moisture-sensitive reagents were performed under nitrogen or argon atmosphere. All microwave-assisted reactions were conducted with a Smith synthesizer from Personal Chemistry (Uppsala, Sweden). Silica gel chromatography was performed using either glass columns packed with silica gel (230−400 mesh) or prepacked silica gel cartridges from Isco. All NMR spectra were collected on a Bruker 360 MHz, 400 or 600 MHz or on a Varian 300 or 400 MHz spectrometer. The chemical shifts were expressed as ppm ($\delta$ units) with tetramethylsilane or residual protonated solvent used as a reference. All tested compounds were purified to ≥95% purity as determined by reverse phase UPLC. UPLC analysis was obtained on a Waters ACQUITY UPLC and UPLC-MS. UPLC method A (2.0 min UPLC run): Acquity UPLC HSS T3 C18 column, 50 mm × 2.1 mm, 1.7 $\mu$m, 35 °C; mobile phase, A = 0.1% TFA in H$_2$O, B = 0.1% TFA in acetonitrile; gradient, 0.0−1.5 min, 5−100% B; flow rate, 1 mL/min; 218 and 254 nM; 1 min post time; 1 $\mu$L injection. UPLC-MS (2.0 min UPLC run): Acquity UPLC HSS T3 C18 column, 50 mm × 2.1 mm, 1.8 $\mu$m, 50 °C; mobile phase, A = 0.05% formic acid + 3.75 mM ammonium acetate in H$_2$O, B = 0.04% formic acid in acetonitrile; gradient, 0.0−1.4 min, 2−100% B; flow rate, 1.2 mL/min; 218 and 254 nM; 1 min post time; 1−5 $\mu$L injection. All assay compounds had a measured purity of ≥95% (by TLC and UV) as determined using analytical UPLC or UPLC-MS system. Low-resolution mass spectral (MS) data were determined on an Agilent 1100 mass spectrometer using ES ionization modes (positive and/or negative) and water−methanol (MeOH) 3:7 + 2% of a 25% ammonium hydroxide solution. High-resolution mass spectral (HRMS) data were determined on a LTQ Orbitrap XL-Thermo Fisher (Germany). Optical rotations were determined with a Perkin-Elmer 241 polarimeter at room temperature and at 589 nm using a sodium lamp and a 1 mL cell. Data were reported as follows: $[\alpha]_D$ (concentration g/100 mL, solvent). Melting points were recorded on a Büchi M-565 apparatus by heating a capillary tube containing the sample at a rate of 0.5−1 °C/min.

*General Method for Preparation of P3 Alkoxy-Substituted Benzyl Sulfone cHEA Inhibitors **60a,b**, **60h**, and **60p,q**: 4-tert-Butoxycarbonylamino-3-oxo-5-tritylsulfanyl-pentanoic Acid Allyl Ester (7).* To a solution of di(1H-imidazol-1-yl)methanone (13.9 g, 84 mmol) in anhydrous THF (300 mL) was added dropwise a solution of (R)-2-((tert-butoxycarbonyl)amino)-3-(tritylthio)propanoic acid (32.8 g, 70 mmol) and 4-(N,N-dimethylamino)pyridine (0.26 g, 2.1 mmol) in THF (200 mL) at 25 °C over a period of 1 h. The reaction mixture was stirred for 2 h at ambient temperature before a solution of propanedioic acid mono-2-propenyl ester magnesium complex (13.6 g, 42 mmol) in THF (200 mL) was added. The reaction mixture was

stirred for 16 h at 40−45 °C and evaporated. The residue was redissolved in ethyl acetate (EtOAc) and washed with cold 10% citric acid, water, aq. NaHCO$_3$, and brine, dried over MgSO$_4$, filtered, and concentrated. The crude material was purified by flash column chromatography (10−25% EtOAc/hexanes) to give after crystallization from diethylether (Et$_2$O)/hexane 24.9 g (65%) of (R)-allyl 4-((tert-butoxycarbonyl)amino)-3-oxo-5-(tritylthio)pentanoate as a white crystalline solid. $^1$H NMR (400 MHz, CDCl$_3$): $\delta$ 7.40 (d, J = 7.4 Hz, 6H), 7.14−7.33 (m, 9H), 5.75−5.96 (m, 1H), 5.16−5.36 (m, 2H), 5.01 (d, J = 7.0 Hz, 1H), 4.57 (d, J = 5.9 Hz, 2H), 4.08 (d, J = 4.7 Hz, 1H), 3.22−3.43 (m, 2H), 2.71 (dd, J = 4.3, 12.9 Hz, 1H), 2.52 (dd, J = 7.2, 12.7 Hz, 1H), 1.43 (s, 9H). LC/MS LC/MS (ESI, negative ion): m/z 544 (M − H).

*(3R*,5R*)-Allyl 5-((tert-butoxycarbonyl)amino)-4-oxotetrahydro-2H-thiopyran-3-carboxylate (8).* To a solution of (R)-allyl 4-((tert-butoxycarbonyl)amino)-3-oxo-5-(tritylthio)pentanoate (24.0 g, 44 mmol) in acetic acid (200 mL) were added piperidine (5.3 g, 61.6 mmol) and para-formaldehyde (1.46 g, 46 mmol), and the reaction mixture was stirred at 80 °C for 0.5 h. The reaction mixture was concentrated under reduced pressure, and the residual solid was dissolved in EtOAc and washed with aq. NaHCO$_3$ and brine, dried over MgSO$_4$, filtered, and concentrated. The crude product was redissolved in 50 mL of CH$_2$Cl$_2$ and after the addition of 5 mL of triethylsilane and 1 mL of trifluoroacetic acid was stirred for 16 h at 25 °C. The reaction mixture was basified with aq. NaHCO$_3$ and separated, and the organics were washed with water, dried over MgSO$_4$, filtered, and concentrated. To the crude product was crystallized from Et$_2$O/hexane to give 3.7 g (86%) of (3R*,5R*)-allyl 5-((tert-butoxycarbonyl)amino)-4-oxotetrahydro-2H-thiopyran-3-carboxylate a white solid: mp 114−115 °C. $^1$H NMR (400 MHz, CDCl$_3$): $\delta$ 5.91 (ddt, J = 17.0, 10.7, 5.9 Hz, 1H), 5.68 (m, 1H), 5.24-5.47 (m, 2H), 4.55−4.75 (m, 3H), 3.87 (dd, J = 12.1, 4.7 Hz, 1H), 3.33 (m, 1H), 3.22 (dd, J = 13.9, 12.3 Hz, 1H), 3.04 (ddd, J = 14.1, 4.7, 3.5 Hz, 1H), 2.68 (t, J = 12.3 Hz, 1H), 1.42 (s, 9H). LC/MS (ESI, positive ion): m/z 314 (M + H). Anal. (C$_{14}$H$_{21}$NO$_5$S) C, H, N.

*3,5-Difluoro-4-nitro-benzonitrile (54).* To a solution of sodium perborate (89 g, 0.548 mol) in acetic acid (800 mL) was added over a period of 2 h a solution of 4-bromo-2,6-difluoroaniline (53) (60.0 g, 0.274 mol) dissolved in acetic acid (600 mL) at 65−70 °C. After addition, the reaction mixture was stirred for 3 h at 65 °C, before an additional amount of sodium perborate (89 g, 0.548 mol) was added in 10 g portions over a period of 4 h. After it was stirred for 14 h at 65 °C, the cold reaction mixture was added to ice−water, and the product was extracted with EtOAc−hexane 1:1. Combined extracts were washed with water, 10% aq. K$_2$CO$_3$ solution, 10% aq. KHSO$_4$ solution, and brine, dried over MgSO4, filtered, and concentrated. Crystallization from Et$_2$O−hexane gave 52.1 g (79%) of 5-bromo-1,3-difluoro-2-nitro-benzene as orange crystals: Anal. (C$_7$H$_2$F$_2$N$_2$O$_2$) C, H, N, F.

To a solution of 5-bromo-1,3-difluoro-2-nitro-benzene (33 g, 138.6 mmol) in N-methyl-pyrrolidone (150 mL) was added the CuCN (16.3 g, 180 mmol), and the resulting suspension was heated under argon at 160−165 °C for 6 h. The reaction mixture was diluted with ice−water, filtered over Celite, and extracted with EtOAc. Combined organic

layers were washed with water, 0.5 N aq. NH$_4$OH, and brine, dried over MgSO$_4$, filtered, and concentrated to obtain after purification by flash column chromatography (5−20% EtOAc in hexane) 20.9 g (82%) of 3,5-difluoro-4-nitro-benzonitrile as a beige crystalline solid: mp 88−89 °C. $^1$H NMR (400 MHz, CDCl$_3$): δ 7.39 (d, J = 6.6 Hz, 2H). Anal. (C$_8$H$_5$F$_2$NO$_4$) C, H, N, F.

*Methyl 3,5-Difluoro-4-nitrobenzoate (55).* Thionylchloride (1.0 mol, 134 mL) was added to MeOH (400 mL) over a period of 0.5 h below 0 °C. To this solution was added 3,5-difluoro-4-nitro-benzonitrile (33.5 g, 180 mmol), and the reaction mixture was stirred overnight at 25 °C. The reaction mixture was slowly warmed up to 50 °C, and the evolving gas was trapped in a gas washer. The reaction mixture was heated for 2 h at reflux and then concentrated. The crude product was redissolved in EtOAc, washed with aq. NaHCO$_3$ solution and brine, dried over MgSO$_4$, filtered, and concentrated to obtain after crystallization from EtOAc−hexane 37.5 g (96%) of methyl 3,5-difluoro-4-nitrobenzoate as yellow crystals: mp 70−72 °C. $^1$H NMR (400 MHz, CDCl$_3$): δ 7.76 (d, 2H), 3.98 (s, 3H).

*5-(Bromomethyl)-1,3-difluoro-2-nitro-benzene (56).* To a solution of methyl 3,5-difluoro-4-nitrobenzoate (18.2 g, 84 mmol) in THF (300 mL) was added under argon at 0−5 °C a 1 M diisobutylaluminium hydride solution in hexane (280 mL, 280 mmol) within 1.5 h. The reaction mixture was stirred for 2.5 h at 0−5 °C and then added to a cold 1 M aq. potassium tartrate solution (200 mL) under ice cooling. After the reaction mixture was stirred for 0.5 h at 25 °C, the aqueous phase was extracted with EtOAc. Combined organic extracts were washed with brine, dried over MgSO$_4$, filtered, and concentrated to provide 15.6 g (98%) of (3,5-difluoro-4-nitrophenyl)methanol as a yellow solid, which was used without further purification. $^1$H NMR (400 MHz, CDCl$_3$) δ 7.12 (d, 2H), 4.77 (s, 2H).

To a solution of PBr$_3$ (10.3 mL, 106.5 mmol) in Et$_2$O (200 mL) was added under argon at 0 °C a solution of (3,5-difluoro-4-nitrophenyl)methanol (15.4 g, 71 mmol) in Et$_2$O (250 mL). The reaction mixture was allowed to warm to 25 °C and was stirred for 24 h at 25 °C. After the addition of MeOH (10 mL) at 0 °C, the reaction mixture was poured onto cold sat. NaHCO$_3$ solution, and the product was extracted with EtOAc. Combined organic extracts were washed with aq. NaHCO$_3$ solution and brine, dried over MgSO$_4$, filtered, and concentrated to provide, after filtration through a plug of silica gel with hexane−EtOAc 3:1, 17.1 g (98%) of 5-(bromomethyl)-1,3-difluoro-2-nitro-benzene as a yellow solid. $^1$H NMR (400 MHz, CDCl$_3$): δ 7.14 (d, 2H), 4.40 (s, 2H).

*tert-Butyl ((3R*,5S*)-5-(3,5-Difluoro-4-nitrobenzyl)-4-oxotetrahydro-2H-thiopyran-3-yl)carbamate (57).* To a solution of 5-bromomethyl-1,3-difluoro-2-nitro-benzene (16.9 g, 67 mmol) in acetone (300 mL) was added allyl 5-((tert-butoxycarbonyl)amino)-4-oxotetrahydro-2H-thiopyran-3-carboxylate (8) (22.4 g, 70.4 mmol) and K$_2$CO$_3$ (23.4 g, 167.5 mmol). The reaction mixture was stirred for 2.5 h at 25−30 °C, filtered, and concentrated. The residual oil was dissolved in EtOAc, washed with brine, dried over MgSO$_4$, filtered, and concentrated. The crude material was dissolved in tert-butyl methyl ether (TBME) (100 mL) and degassed with argon and then added to a degassed solution of triethylamine (23.2 mL, 167.5 mmol), formic acid (4.9 mL, 127.3 mol), PPh$_3$ (0.88 g, 3.34 mmol), and palladium(II) acetate [Pd(OAc)$_2$] (0.60 g, 2.6 mmol) in TBME (150 mL), and the reaction mixture was stirred for 16 h at 25 °C to allow complete equilibration to the desired (3R,5S)-diastereoisomer. The reaction mixture was poured into aq. KHSO$_4$ solution and was extracted with methyl-tert-butylether. Combined organic extracts were washed with aq. NaHCO$_3$ solution and brine, dried over MgSO$_4$, filtered, and concentrated. The crystallized product was recrystallized from methyl-tert-butylether-hexane to provide 18.9 g (77%) of tert-butyl ((3R*,5S*)-5-(3,5-difluoro-4-nitrobenzyl)-4-oxotetrahydro-2H-thiopyran-3-yl)carbamate as white crystals: mp 158−159 °C. $^1$H NMR (400 MHz, CDCl$_3$): δ 6.94 (d, J = 8.6 Hz, 1H), 5.69 (m, 1H), 4.55 (m, 1H), 3.40 (m, 1H), 3.23 (dd, J = 14.5, 7.8 Hz, 1H), 3.11 (m, 1H), 2.83 (ddd, J = 13.3, 4.7, 3.5 Hz, 1H), 2.55−2.75 (m, 3H), 1.43 (s, 9H). LC/MS (ESI, positive ion): m/z 420 (M + H + NH$_3$). Anal. (C$_{17}$H$_{20}$F$_2$N$_2$O$_5$S) C, H, N, F.

*((3R,4S,5S)-5-(3,5-Difluoro-4-nitrobenzyl)-4-hydroxy-1,1-dioxido-tetrahydro-2H-thiopyran-3-yl)carbamate (58).* To a suspension of LiAlH$_4$ (4.88 g, 128 mmol) in THF (300 mL) was added under argon a solution of tert-butyl ((3R*,5S*)-5-(3,5-difluoro-4-nitrobenzyl)-4-oxotetrahydro-2H-thiopyran-3-yl)carbamate (47.0 g, 117 mmol) in THF (400 mL) below −70 °C over a period of 2 h. After it was stirred for 1 h at −78 °C, the reaction was sequentially quenched with 5 mL of H$_2$O in 20 mL of THF at 0−5 °C, 5 mL of 4 N NaOH, and, after it was stirred for 30 min, an additional with 15 mL of H$_2$O. The reaction mixture was stirred for 1 h, then dried with MgSO$_4$, filtered over Celite, and concentrated. The product was recrystallized twice from ethanol (EtOH) to obtain 26.8 g (54%) of the [(3R*,4S*,5S*)-diastereoisomer as white crystals. The racemic product was separated using a Chiralpak AY column (7.6 cm × 25 cm, n-heptane-EtOH 1:1) to provide 12.9 g (29%) of the undesired ((3S,4R,5R)-5-(3,5-difluoro-4-nitrobenzyl)-4-hydroxy-1,1-dioxidotetrahydro-2H-thiopyran-3-yl)-carbamate (peak 2) and 13.2 g (30%) of the desired ((3R,4S,5S)-5-(3,5-difluoro-4-nitrobenzyl)-4-hydroxy-1,1-dioxidotetrahydro-2H-thio-pyran-3-yl)carbamate in >99.8% enantiomeric excess (ee) (peak 1, [α]$_D$ −0.374, c = 1, CHCl$_3$) as colorless solids: mp 205−207 °C. $^1$H NMR [600 MHz, dimethyl sulfoxide (DMSO)-d$_6$]: δ 7.33 (d, J = 9.9 Hz, 2H), 6.73 (d, J = 8.1 Hz, 1H), 4.92 (d, J = 6.9 Hz, 1H), 3.39 (m, 1H), 3.20 (dd, J = 13.3, 3.2 Hz, 1H), 2.90 (dt, J = 10.1, 7.5 Hz, 1H), 2.54 (dd, J = 13.3, 9.3 Hz, 1H), 2.38 (dd, J = 12.7, 11.7 Hz, 1H), 2.29 (d, J = 13.9 Hz, 1H), 2.25 (ddd, J = 13.5, 11.5, 1.8 Hz, 1H), 1.94 (m, 1H), 1.38 (s, 9H). LC/MS (ESI, positive ion): m/z 349 (M + H-isobutylene).

*(3R,4S,5S)-3-((3-(tert-Butyl)benzyl)amino)-5-(3,5-difluoro-4-nitro-benzyl)-4-hydroxytetrahydro-2H-thiopyran 1,1-Dioxide (59).* To a solution of ((3R,4S,5S)-5-(3,5-difluoro-4-nitrobenzyl)-4-hydroxy-1,1-dioxidotetrahydro-2H-thiopyran-3-yl)carbamate (12.3 g, 29.4 mmol) in THF−water 1:1 (350 mL) was added potassium peroxomonosulfate (39.2 g, 61.8 mmol), and the reaction mixture was stirred for 2 h at 40 °C. Excess potassium peroxomonosulfate was destroyed with sodium metabisulfite (12 g). The reaction mixture was stirred for 0.5 h and basified with aq. K$_2$CO$_3$ solution, and the product was extracted with EtOAc. Combined organic extracts were washed with brine, dried over MgSO$_4$, filtered, and concentrated to provide after crystallization from THF−hexane 12.1 g (94%) of (3R,4S,5S)-3-((3-(tert-butyl)benzyl)-amino)-5-(3,5-difluoro-4-nitrobenzyl)-4-hydroxytetrahydro-2H-thio-pyran 1,1-dioxide as yellow crystals. $^1$H NMR (600 MHz, DMSO-d$_6$): δ 7.32 (d, J = 9.9 Hz, 2H), 6.91 (d, J = 8.6 Hz, 1H), 5.24 (d, J = 7.7 Hz, 1H), 3.73 (m, 1H), 2.99−3.20 (m, 5H), 2.93 (dt, J = 14.6, 3.7 Hz, 1H), 2.74 (dd, J = 13.1, 8.2 Hz, 1H), 2.18 (m, 1H), 1.38 (s, 9H). LC/MS (ESI, positive ion): m/z 454 (M + H).

To (3R,4S,5S)-3-((3-(tert-butyl)benzyl)amino)-5-(3,5-difluoro-4-nitrobenzyl)-4-hydroxytetrahydro-2H-thiopyran 1,1-dioxide (8.6 g, 20 mmol) was added 4 N HCl in dioxane (20 mL), and the reaction mixture was stirred for 2 h at 25 °C. After evaporation to dryness, the residue was stirred in diisopropylether for 1 h, filtered, and dried at 50 °C under reduced pressure to provide 7.4 g (99%) of (3R,4S,5S)-3-amino-5-(3,5-difluoro-4-nitrobenzyl)-4-hydroxytetrahydro-2H-thiopyr-an 1,1-dioxide hydrochloride as a white solid. $^1$H NMR (600 MHz, DMSO-d$_6$): δ 8.26 (br s, 3H), 7.37 (d, J = 10.1 Hz, 2H), 6.11 (d, J = 8.2 Hz, 1H), 3.36−3.44 (m, 3H), 3.32 (m, 1H), 3.24 (t, J = 14.0 Hz, 1H), 3.14 (dd, J = 13.3, 3.9 Hz, 1H), 3.07 (br d, J = 14.0 Hz, 1H), 2.74 (dd, J = 13.4, 8.4 Hz, 1H), 2.27 (m, 1H). LC/MS (ESI, positive ion): m/z 337 (M + H). Anal. (C$_{12}$H$_{15}$ClF$_2$N$_2$O$_5$S) C, H, N, S.

To a solution of (3R,4S,5S)-3-amino-5-(3,5-difluoro-4-nitrobenzyl)-4-hydroxytetrahydro-2H-thiopyran 1,1-dioxide hydrochloride (1.45 g, 3.9 mmol) in MeOH−CH$_2$Cl$_2$ 1:1 (30 mL) were added sodium acetate (NaOAc) (0.734 g, 8.5 mmol) and 3-tert-butyl-benzaldehyde (0.64 g, 3.9 mmol), and the reaction mixture was stirred for 0.5 h at 25 °C before NaBH$_3$CN (0.40 g, 5.8 mmol) was added followed by stirring for 1 h. The reaction mixture was acidified with 1 N HCl, stirred for 15 min, basified with aq. K$_2$CO$_3$ solution, and extracted with EtOAc. The combined organic layers were washed with brine, dried over MgSO$_4$, filtered through a plug of silica gel, and concentrated to provide after crystallization from THF/diisopropylether 1.82 g (97%) of (3R,4S,5S)-3-((3-(tert-butyl)benzyl)amino)-5-(3,5-difluoro-4-nitro-

benzyl)-4-hydroxytetrahydro-2*H*-thiopyran 1,1-dioxide as a light yellow solid: mp 198−200 °C. ¹H NMR (600 MHz, DMSO-*d*₆): δ 7.34 (m, 3H), 7.21−7.26 (m, 2H), 7.13 (dt, *J* = 6.8, 1.4 Hz, 1H), 5.30 (d, *J* = 6.11 Hz, 1H), 3.81 (d, *J* = 13.3 Hz, 1H), 3.63 (d, *J* = 13.3 Hz, 1H), 3.38 (ddd, *J* = 14.4, 4.2, 3.5 Hz, 1H), 3.13−3.20 (m, 1H), 3.09 (dd, *J* = 13.3, 4.0 Hz, 1H), 3.03 (t, *J* = 13.6 Hz, 1H), 2.97 (dd, *J* = 13.4, 11.7 Hz, 1H), 2.89 (dt, *J* = 14.5, 3.7 Hz, 1H), 2.79 (m, 1H), 2.74 (dd, *J* = 13.3, 8.2 Hz, 1H), 2.41 (br s, 1H), 2.16 (m, 1H). LC/MS (ESI, positive ion): *m/z* 483 (M + H). Anal. (C₂₃H₂₈F₂N₂O₅S) C, H, N, S, F.

*(3R,4S,5S)-3-(4-Amino-3-fluoro-5-propoxybenzyl)-5-((3-(tert-butyl)benzyl)amino)-4-hydroxytetrahydro-2H-thiopyran 1,1-Dioxide Dihydrochloride (60a).* To a suspension of (3*R*,4*S*,5*S*)-3-((3-(*tert*-butyl)benzyl)amino)-5-(3,5-difluoro-4-nitrobenzyl)-4-hydroxytetrahydro-2*H*-thiopyran 1,1-dioxide (0.126 g, 0.26 mmol) in THF (1.0 mL) were added *n*-propanol (1.0 mL) and pulverized KOH (0.016 g, 0.28 mmol), and the resulting reaction mixture was heated in the microwave for 40 min at 90 °C. The reaction mixture was diluted with EtOAc and washed with brine, dried over MgSO4, filtered, and concentrated. The crude product was dissolved MeOH (5 mL) and after addition of 10% Pd−C (30 mg) stirred under atmospheric H₂ for 5 h at 50 °C. The catalyst was filtered off over Celite, and the filtrate was concentrated. The crude product was converted into the dihydrochloride salt in CH₂Cl₂ with 2 equiv of 1 N HCl in Et₂O, evaporated, and crystallized from acetonitrile−Et₂O to provide 0.114 g (77%) of (3*R*,4*S*,5*S*)-3-(4-amino-3-fluoro-5-propoxybenzyl)-5-((3-(*tert*-butyl)benzyl)amino)-4-hydroxytetrahydro-2*H*-thiopyran 1,1-dioxide dihydrochloride as a white solid. ¹H NMR (400 MHz, CD₃OD): δ 7.63 (s, 1H), 7.53 (d, *J* = 7.6 Hz, 1H), 7,42 (t, *J* = 7.6 Hz, 1H), 7.36 (m, 1H), 6.86 (s, 1H), 6.80 (d, *J* = 10.5 Hz, 1H), 4.39 (d, *J* = 13.3 Hz, 1H), 4.30 (d, *J* = 13.3 Hz, 1H), 4.12 (t, *J* = 6.6 Hz, 2H), 3.80 (t, *J* = 10.2 Hz, 1H), 3.55−3−75 (m, 2H), 3.50 (m, 1H), 3.36 (dd, *J* = 13.7, 2.7 Hz, 1H), 3.19 (t, *J* = 14.2 Hz, 1H), 2.78 (dt, *J* = 14.4, 3.2 Hz, 1H), 2.53 (dd, *J* = 11.7, 10.5 Hz, 1H), 2.27 (m, 1H), 1.88 (m, 2H), 1.35 (m, 9H), 1.07 (t, *J* = 7.2 Hz, 3H). LC/MS (ESI, positive ion): *m/z* 493 (M + H). HRMS *m/z* 493.25351 [(M + H)⁺ calcd for C₂₆H₃₈N₂O₄FS⁺, 493.25308].

*(3S,4S,5R)-3-(4-Amino-3-ethoxy-5-fluorobenzyl)-5-((3-(tert-butyl)benzyl)amino)-4-hydroxytetrahydro-2H-thiopyran 1,1-Dioxide Dihydrochloride (60b).* To a suspension of (3*R*,4*S*,5*S*)-3-((3-(*tert*-butyl)benzyl)amino)-5-(3,5-difluoro-4-nitrobenzyl)-4-hydroxytetrahydro-2*H*-thiopyran 1,1-dioxide (0.30 g, 0.61 mmol) in THF (3 mL) were added EtOH (1.5 mL) and pulverized KOH (0.038 g, 0.65 mmol), and the resulting reaction mixture was heated in the microwave for 20 min at 90 °C. The solvent was removed under reduced pressure, and (3*R*,4*S*,5*S*)-3-((3-(*tert*-butyl)benzyl)amino)-5-(3-ethoxy-5-fluoro-4-nitrobenzyl)-4-hydroxytetrahydro-2*H*-thiopyran 1,1-dioxide was obtained as a yellow foam suitable for use in the next step. ¹H NMR (400 MHz, CDCl₃): δ 7.3 (m, 3H), 7.12 (d, *J* = 7.0 Hz, 1H), 6.47 (d, *J* = 10.9 Hz, 1H), 6.39 (s, 1H), 4.0−4.1 (m, 3H), 3.90 (dd, *J* = 12.9 Hz, 1H), 3.76 (d, *J* = 12.9 Hz, 1H), 3.66−3.73 (m, 2H), 3.39 (dt, *J* = 13.7, 3.1 Hz, 1H), 2.6−3.2 (m, 6H), 2.41 (m, 1H), 1.41 (t, *J* = 7.0 Hz, 3H), 1.33 (s, 9H). LC/MS (ESI, positive ion): *m/z* 509 (M + H).

To a solution of (3*R*,4*S*,5*S*)-3-((3-(*tert*-butyl)benzyl)amino)-5-(3-ethoxy-5-fluoro-4-nitrobenzyl)-4-hydroxytetrahydro-2*H*-thiopyran 1,1-dioxide (0.33 g, 0.60 mmol) in MeOH (10 mL) was added NiCl₂−6H₂O (0.146 g, 0.60 mmol) and at 0−5 °C NaBH₄ (0.093 g, 2.40 mmol) in small portions over a period of 15 min. After it was stirred for 2 h at 0−5 °C, the reaction was quenched with 0.5 mL of H₂O. The reaction mixture was filtered through a plug of Celite and concentrated. The crude product was purified by reverse-phase preparative HPLC to afford after crystallization of dihydrochloride salt from acetonitrile−Et₂O 0.198 g (59%) of (3*S*,4*S*,5*R*)-3-(4-amino-3-ethoxy-5-fluorobenzyl)-5-((3-(*tert*-butyl)benzyl)amino)-4-hydroxytetrahydro-2*H*-thiopyran 1,1-dioxide dihydrochloride as a white crystalline solid. ¹H NMR (600 MHz, DMSO-*d*₆): δ 10.07 (br s, 1H), 9.10 (br s, 1H), 7.69 (s, 1H), 7.44 (d, *J* = 7.7 Hz, 1H), 7.33−7.42 (m, 2H), 6.60−6.67 (m, 2H), 6.25 (br s, 1H), 4.18−4.30 (m, 2H), 4.02−4.13 (m, 2H), 3.90 (dt, *J* = 13.7, 3.2 Hz, 2H), 3.61−3.71 (m,

2H), 3.17 (m, 2H), 3.05 (dd, *J* = 13.7, 3.0 Hz, 1H), 2.82 (dt, *J* = 14.7, 3.4 Hz, 1H), 2.43 (dd, *J* = 13.3, 9.3 Hz, 1H), 2.04 (m, 1H), 1.35 (t, *J* = 7.0 Hz, 3H), 1.30 (m, 9H). LC/MS (ESI, positive ion): *m/z* 479 (M + H). HRMS *m/z* 479.23752 [(M + H)⁺ calcd for C₂₅H₃₅FN₂O₄S⁺, 479.23743]. Anal. (C₂₅H₃₇ClFN₂O₄S) C, H, N, F, S.

*(3S,4S,5R)-3-(4-Amino-3-fluoro-5-(2,2,2-trifluoroethoxy)benzyl)-5-((3-(tert-butyl)benzyl)amino)-4-hydroxytetrahydro-2H-thiopyran 1,1-Dioxide Dihydrochloride (60h).* Using 2,2,2-trifluoro-ethanol and (3*R*,4*S*,5*S*)-3-((3-(*tert*-butyl)benzyl)amino)-5-(3,5-difluoro-4-nitrobenzyl)-4-hydroxytetrahydro-2*H*-thiopyran 1,1-dioxide (59) and following the procedures used to prepare 60b gave 60h. ¹H NMR (600 MHz, DMSO-*d*₆): δ 9.92 (br s, 1H), 9.06 (br s, 1H), 7.68 (s, 1H), 7.45 (d, *J* = 7.5 Hz, 1H), 7.34−7.42 (m, 2H), 6.77 (d, *J* = 8.3 Hz, 1H), 6.60−6.70 (m, 1H), 6.25 (br s, 1H), 4.65−4.84 (m, 2H), 4.13−4.34 (m, 2H), 3.87 (dt, *J* = 13.7, 3.6 Hz, 1H), 3.72 (br s, 1H), 3.58−3.68 (m, 2H), 3.08−3.22 (m, 2H), 3.01 (dd, *J* = 13.5, 3.0 Hz, 1H), 2.85 (td, *J* = 14.3, 3.4 Hz, 1H), 2.40 (dd, *J* = 13.4, 9.0 Hz, 1H), 2.02 (m, 1H), 1.27 (m, 9H). LC/MS (ESI, positive ion): *m/z* 533 (M + H). HRMS *m/z* 533.20936 [(M + H)⁺ calcd for C₂₅H₃₂F₄N₂O₄S⁺, 533.20917].

*(3S,4S,5R)-3-(4-Amino-3-fluoro-5-(((R)-1,1,1-trifluoro-3-methoxypropan-2-yl)oxy)benzyl)-5-((3-(tert-butyl)benzyl)amino)-4-hydroxytetrahydro-2H-thiopyran 1,1-Dioxide Dihydrochloride (60p).* Using (*R*)-1,1,1-trifluoro-3-methoxy-propan-2-ol and (3*R*,4*S*,5*S*)-3-((3-(*tert*-butyl)benzyl)amino)-5-(3,5-difluoro-4-nitrobenzyl)-4-hydroxytetrahydro-2*H*-thiopyran 1,1-dioxide (59) and following the procedures used to prepare 60b gave 60p. ¹H NMR (600 MHz, DMSO-*d*₆): δ 10.06 (br s, 1H), 9.11 (br s, 1H), 7.69 (br s, 1H), 7.44 (d, *J* = 7.7 Hz, 1H), 7.41 (d, *J* = 7.3 Hz, 1H), 7.37 (t, *J* = 7.7 Hz, 1H), 6.78 (s, 1H), 6.78 (m, 1H), 6.70 (d, *J* = 11.1 Hz, 1H), 6.26 (br s, 1H), 5.17 (m, 1H), 4.24−4.30 (m, 2H), 4.17−4.24 (m, 1H), 3.89 (m, 2H), 3.62−3.79 (m, 4H), 3.32 (s, 3H), 3.12−3.22 (m, 2H), 3.04 (dd, *J* = 13.5, 2.6 Hz, 1H), 2.35 (dd, *J* = 13.4, 9.6 Hz, 1H), 1.93−2.06 (m, 1H), 1.29 (s, 9H). LC/MS (ESI, positive ion): *m/z* 577 (M + H). HRMS *m/z* 577.23537 [(M + H)⁺ calcd for C₂₆H₃₁F₇N₂O₄S⁺, 577. 23528].

*(3S,4S,5R)-3-(4-Amino-3-fluoro-5-(((R)-1,1,1-trifluoro-3-(2-methoxyethoxy)propan-2-yl)oxy)benzyl)-5-((3-(tert-butyl)benzyl)amino)-4-hydroxytetrahydro-2H-thiopyran 1,1-Dioxide Dihydrochloride (60q).* Using (*R*)-1,1,1-trifluoro-3-(2-methoxy−ethoxy)-propan-2-ol and (3*R*,4*S*,5*S*)-3-((3-(*tert*-butyl)benzyl)amino)-5-(3,5-difluoro-4-nitrobenzyl)-4-hydroxytetrahydro-2*H*-thiopyran 1,1-dioxide (59) and following the procedures used to prepare 60m gave 60q. ¹H NMR (600 MHz, DMSO-*d*₆): δ 10.09 (br s, 1H), 9.12 (br s, 1H), 7.70 (s, 1H), 7.44 (d, *J* = 7.5 Hz, 1H), 7.41 (d, *J* = 7.5 Hz, 1H), 7.37 (t, *J* = 7.6 Hz, 1H), 6.79 (s, 1H), 6.71 (d, *J* = 11.1 Hz, 1H), 5.15 (m, 1H), 4.66 (br s, 2H), 4.17−4.31 (m, 2H), 3.79−3.93 (m, 3H), 3.70 (d, *J* = 9.7 Hz, 1H), 3.67 (d, *J* = 13.5 Hz, 1H), 3.58−3.63 (m, 2H), 3.42 (t, *J* = 4.5 Hz, 2H), 3.12−3.22 (m, 5H), 3.06 (m, 2H), 2.77 (dt, *J* = 14.7, 2.8 Hz, 1H), 2.34 (dd, *J* = 13.4, 9.6 Hz, 1H), 2.00 (m, 1H), 1.29 (s, 9H). LC/MS (ESI, positive ion): *m/z* 621 (M + H). HRMS *m/z* 621.26153 [(M + H)⁺ calcd for C₂₉H₄₁F₄N₂O₆S⁺, 621.26160].

**BACE1 Enzymatic Assay.** Human BACE1 activity was assayed using recombinant BACE1 ectodomain in 100 mM acetate buffer, pH 4.5, containing 0.1% CHAPS and a synthetic fluorescence-quenched peptide substrate (3 μM, equal to 0.17 $K_M$). Test substances were serially diluted from 10 μM to 0.6 nM, and inhibition assays were done in black 96-well plates (Corning), with a final DMSO concentration of 5%. BACE1 and inhibitors were incubated in assay buffer at room temperature for 1 h, and residual enzymatic activity was measured after the addition of substrate in a Spectramax Gemini fluorescence plate reader (Molecular Devices, Sunnyvale, CA) for 15 min. $IC_{50}$ values were calculated using the Microsoft Excel extension XL-fit. Each compound was tested on duplicate plates, in two independent experiments.

**CatD Enzymatic Assay.** The activity of human recombinant CatD was measured in 100 mM acetate buffer, pH 4.5, with Mca-GKPILFFRLK(DNP)-*d*R-NH₂ (2 μM, Bachem, Bubendorf, Switzerland). Test substances were serially diluted from 10 μM to 0.6 nM, and inhibition assays were done in black 96-well plates (Costar) with a final DMSO concentration of 5%. CatD and inhibitors were incubated in assay buffer at room temperature for 1 h, and the residual enzymatic

activity was measured after the addition of substrate in a Spectramax Gemini fluorescence plate reader (Molecular Devices) for 15 min. $IC_{50}$ values were calculated using the Microsoft Excel extension XL-fit. Each compound was tested on duplicate plates, in two independent experiments.

**Cell-Based Assay for Determination of $IC_{50}$s for A$\beta$40 in CHO APPwt Cells.** Chinese hamster ovary cells stably transfected with the gene for human amyloid precursor protein were plated at a density of 6000 cells/well into 96-well microtiter plates and cultivated for 24 h in DMEM cell culture medium containing 10% FCS. The test compound was added to the cells at a concentration ranging from 10 $\mu$M to 3 nM, and the cells were cultivated for 24 h. The supernatants were collected, and the concentration of amyloid peptide 1−40 was determined using an in-house homogeneous time-resolved fluorescence (HTRF) immunoassay. The $IC_{50}$ was calculated from the percentage of inhibition of amyloid peptide release as a function of the test compound concentration. Each compound was tested in three independent experiments.

**Permeability Assay.** Bidirectional transport was examined in MDCK cells stably expressing MDR1 (Madin−Darby Canine Kidney cells retrovirally transduced with the human multidrug resistance gene 1-(P-gP) to assess permeation and P-gp-mediated efflux of BACE1 inhibitors. After the cells were seeded on transwells for at least 3 days, bidirectional transport was examined at 5 $\mu$M after a 2 h of incubation at 37 °C. Levels of BACE1 inhibitors in the samples were quantified using LC/MS. The apparent permeability coefficient ($P_{app}$) of tested compounds was estimated from the slope of a plot of cumulative amount of the agent versus time based on the following equation:

$$P_{app} = (dQ/dt)/(A \cdot C_0)$$

where $dQ/dt$ is the penetration rate of the agent (ng/s), $A$ is the surface area of the cell layer on the transwell (0.11 cm$^2$), and $C_0$ is the initial concentration of the test compound (ng/mL). The ER was calculated from the basolateral-to-apical permeability divided by the apical-to-basolateral permeability (ER = $P_{app\ B>A}/P_{app\ A>B}$) to determine the extent of active efflux by P-gp. An increasing ER in MDCK-MDR1 cells is indicative of increasing susceptibility to P-gp.

**Animal Experiments.** All animals were maintained under standard housing conditions with access to standard pelleted food and water ad libitum, including throughout experiments. Animal experiments were conducted in accordance with Swiss national animal welfare regulations, under the ethically approved animal experimentation licenses authorized by the Cantonal Veterinary Authority of Basel city and the Federal Veterinary Office of Switzerland.

**PD Assay.** For efficacy testing in vivo, APP51/16 [B6,D2-Tg(Thy1APP)51/16Npa] transgenic mice were used, which express human APP751 wild-type under the control of a murine Thy-1 expression cassette. The mice were maintained on a C57BL/6 genetic background and were hemizygous for the transgene. Mice were dosed orally by gavage (10 mL/kg) and euthanized 4 h thereafter by decapitation. Blood was collected from the trunk cut. Brains were removed and dissected down the midline. One half-brain was used for pharmacokinetic analysis, the other forebrain (olfactory bulb, cerebellum, and brain stem removed) was used for PD analyses. Samples were immediately frozen on dry ice and stored at −80 °C until use.

Frozen forebrains were subsequently homogenized in 10 volumes (w/v) of TBS with protease inhibitors, extracted with 1% TX-100, and centrifuged at 100000 rpm for 30 min at 4 °C as previously described.[19] The supernatants were analyzed for A$\beta_{40}$ with the 96-well MULTI-ARRAY Human (6E10) Abeta 40 Ultrasensitive Kit (catalog #K111FTE-3, MSD, Gaithersburg, United States). The assay was done according to the manufacturer's instructions. Calibration curves were prepared in nontransgenic 1% TX-100 brain extracts spiked with synthetic A$\beta_{1-40}$ peptide (H-1194.1000, Bachem, Basel, Switzerland) solubilized in water-free DMSO (41647, Fluka). C99 was quantified as described previously.[19] Briefly, forebrain homogenates were dephosphorylated and separated on 13% Tris-bicine gels, and proteins were transferred to Immobilin-P membranes. Blots were probed with antibody APP-C8 against the APP carboxy terminus and processed for

chemiluminescence. Following detection on X-ray films, the band intensities were digitized for quantification. An extract from an APP51/16xBACE1-KO mouse diluted in an APP-KO mouse extract was used as standard. A$\beta_{40}$ and C99 data were statistically analyzed by two-tailed Student's $t$ test, to compare the effect of compound treatments against the respective vehicle-treated controls.

**Pharmacokinetic Assays.** *Cassette Experiment for Early Brain/Blood Ratio Determination.* To gain insights on the brain penetration of newly synthesized compounds, in a timely fashion and with a high throughput, a screening cassette approach was validated and implemented: adult male C57Bl/6 mice (from Iffa-Credo, France), weighing between 20 and 30 g, were used for brain penetration screening studies. The dosing regimen consisted of administering intravenously a mixture of five test compounds at a dose of 0.5 $\mu$mol/kg for each compound. To test the reliability of the cassette dosing within a series of similar compounds, a reference compound was always included in the compound set. The compounds were separately solubilized in *N*-methyl pyrrolidone (NMP), then mixed together, and finally diluted in blank plasma. The final formulation was a mixture of NMP/blank plasma 10/90 (v/v), and the volume of administration was 5 mL/kg body weight. The mice were sacrificed by decapitation at different time points (i.e. at 5 min and 1 and 4 h after intravenous dosage). Trunked-blood was collected into an EDTA-coated Eppendorf tube. For each time point investigated, the brains were removed and immediately frozen on dry ice. Blood and brain samples were stored at −20 °C until analysis.

*Full Pharmacokinetic Studies.* For iv injection, 2 $\mu$mol/kg (∼1 mg/kg) BACE inhibitor was formulated in NMP/blank plasma (10:90 v/v). The compounds were administered to male C57BL/6 mice via injection in the saphenous vein (under light anesthesia) to deliver a final dose volume of 5 mL/kg in each mouse. Blood was collected by sublingual bleeding (∼70 $\mu$L/mouse) or at sacrifice (∼300 $\mu$L/mouse) at 5 and 30 min and 1, 2, 4, 6, and 8 h postdose and brain at 5 min and 1, 4, and 8 h postdose (∼200 mg/mouse), $n$ = 3 mice/sampling time/ route. For oral dosing, 6 (∼3 mg/kg) and 60 $\mu$mol/kg (∼30 mg/kg) BACE inhibitor was dissolved/suspended in carboxymethylcellulose 0.5% w/v in water/Tween 80, 99.5/0.5, v/v. The compounds were administered to male C57BL/6 mice by oral gavage to deliver a final dose volume of 10 mL/kg. Blood was collected at 0.25, 0.5, 1, 2, 4, and 6 h postdose and brain at 1 and/or 4 h postdose.

*Bioanalytical Method.* All blood and brain samples were analyzed for test compound content with LC-MS/MS methodologies by the bioanalytical group within the Department of Metabolism and Pharmacokinetics at Novartis. Specific assay conditions were dependent upon the structural characteristics of test compounds. Briefly, an aliquot of each blood sample was extracted by acetonitrile precipitation. Likewise, brain samples were homogenized with water, and an aliquot of each homogenate was extracted by acetonitrile precipitation. Quantitative analysis was performed on the supernatants using a LC-MS/MS detection method optimized for the group of analytes. Data were reported as quantitative drug concentrations as determined by standard calibration curve analysis, using linear fitting of a weighted plot of the analyte/internal standard peak area ratio versus analyte concentration. Using optimized conditions, the typical lower limit of quantitation achieved was 0.4 ng/mL.

*PK Data Analysis.* To estimate the absorption and disposition parameters of the tested compounds in mice, the blood or plasma concentration versus time profiles after oral and intravenous administration were analyzed by noncompartmental approach, using the WinNonlin program (WinNonlin Pro, version 4.1, Pharsight Corporation, Mountain View, CA) with a weighting factor of $1/Y$. The terminal phase rate constant was determined by choosing at least, but not limited to, three points from the log−linear regression of the terminal portion of the concentration versus time curve. Oral bioavailability (% $F$) was calculated by dividing the dose-normalized AUC from the oral study segment by the dose-normalized AUC from the iv study segment and multiplying by 100.

*X-ray Analysis.* The catalytic domain of human BACE1 was expressed in *E. coli* and refolded, as already described.[54] The crystal structures of the complexes with **3**, **14d**, **32a**, **48**, and **60n** were obtained by soaking orthorhombic crystals of unliganded BACE1, grown at 19 °C from 15% polyethylene glycol (PEG) 1500 in water by the method of vapor diffusion in hanging drop using 7.2–13 mg/mL BACE1 (residues 14−447) in 10 mM Tris-HCl, pH 7.4, 25 mM NaCl. The soaking buffer was 28.5−30.0% PEG 1500, 50 mM sodium citrate, pH 5.2−5.5, with 1.0 mM compound and 1.8% DMSO. For **32a** and **60n**, virtually identical structures were also derived from monoclinic crystals obtained by cocrystallization in 1.0 M ammonium sulfate, using 7.2−8.1 mg/mL BACE1 (residues 14−447) in 10 mM Tris-HCl, pH 7.4, 25 mM NaCl, with a 5.5−6.0-fold excess of compound and 1.8% DMSO. The structure of the complex with **39a** was derived from a cocrystallization experiment in 0.2 M sodium citrate, pH 6.5, 0.2 M sodium iodide, 25% PEG 5000 MME, using 9.8 mg/mL BACE1 (residues 14−453) in 10 mM Tris-HCl, pH 7.4, 25 mM NaCl.

Crystals from soaking experiments were directly flash frozen, and diffraction data were collected either at the Swiss Light Source (SLS, in Villigen, Switzerland) beamline X10SA, with a MAR CCD 225 (**14d**, **60n**) or Pilatus (**3**, **32a**) detector, or in the laboratory (**48**), using a FR-E superbright rotating anode X-ray generator and a MAR345 DTB imaging plate detector. Crystals obtained by cocrystallization in 1.0 M ammonium sulfate were briefly transferred in 1.2 M ammonium sulfate, 25% glycerol, and 1.0 mM compound, before flash freezing and data collection, using either the home source equipped with a MAR345 DTB imaging plate (**32a**) or the MAR CCD 225 detector of the SLS beamline X10SA (**60n**). For the crystals of the complex with **39a**, a 80:20 mix of the reservoir solution with glycerol, containing 1.0 mM compound, was used as a cryoprotectant, and diffraction data were collected at the SLS beamline X10SA using a MAR CCD 225 detector.

All diffraction data were processed with HKL2000[55] (**39a**, **32a** cocrystal) or with XDS[56] as implemented in APRV[57] (**3**, **14d**, **32b** soak, **48**, and **60n** cocrystal and soak). For all diffraction data sets, data completeness was greater than 95%, and $R$ merge was in the 4.6−6.8% range, except for **39a** (9.9%). The diffraction data from soaking experiments (**3**, **14d**, **32a**, **48**, and **60n**) extended to between 1.48 and 1.77 Å, while those from the cocrystallization experiments extended to 2.07 (**60n**), 2.40 (**32a**), and 2.65 Å (**39a**), respectively. All structures were determined by difference Fourier and refined using CNX[58] and Coot,[59] to crystallographic $R$ factors ranging from 17.6 to 20.7% (free $R$ factors ranging between 20.0 and 24.7%).

## ■ ASSOCIATED CONTENT

### ● Supporting Information

Experimental procedures and analytical data for compounds **10−15**, **17**, **18**, **20−24**, **26**, **27**, **29a−32c**, **34−49**, **51**, **52**, and **61−62i**. This material is available free of charge via the Internet at http://pubs.acs.org.

### Accession Codes

New protein/ligand coordinates have been deposited in the PDB with the following accession codes: 3VEU (**3**), 3VF3 (**14d**), 3VG1 (**32a**, soak), 4D83 (**32a**, cocrystallization), 4D85 (**39a**), 4D88 (**48**), 4D89 (**60n**, soak), and 4D8C (**60n**, cocrystallization).

## ■ AUTHOR INFORMATION

### Corresponding Author

*Tel: +41 61 6963255. E-mail: heinrich.rueeger@novartis.com.

### Notes

The authors declare no competing financial interest.
The graphics were created with the PyMOL Molecular Graphics System, version 1.2R; DeLano Scientific: Palo Alto, CA; http://www.pymol.org.

## ■ ABBREVIATIONS USED

aq, aqueous; DME, 1,2-dimethoxyethane; DBU, 1,8-diazabicycloundec-7-ene; DMSO, dimethyl sulfoxide; equiv, equivalent; EDC, 1-ethyl-3-(3-dimethylaminopropyl)carbodiimide; ee, enantiomeric excess; $Et_2O$, diethylether; EtOAc, ethyl acetate; EtOH, ethanol; ER, efflux ratio; HOAt, 1-hydroxy-7-azabenzotriazole; MeOH, methanol; NaOAc, sodium acetate; NMP, *N*-methyl pyrrolidone; $PdCl_2(dppf)$, 1,2,3,4,5-pentaphenyl-1′-(di-*tert*-butylphosphino)ferrocene; $Pd(PPh_3)_4$, tetrakis-(triphenylphosphine)palladium; $Pd_2(dba)_3$, *tris*(dibenzylideneacetone)dipalladium; $Pd(OAc)_2$, palladium-(II) acetate; PEG, polyethylene glycol; PEG MME, polyethylene glycol monomethylether; *i*-PrOH, 2-propanol; SAR, structure−activity relationship; sat, saturated; TBME, *tert*-butyl methyl ether; THF, tetrahydrofuran; Trt, trityl; Ts, tosyl

## ■ REFERENCES

(1) Davis, K. L.; Samuels, S. C. Dementia and delerium. In *Pharmacological Management of Neurological and Psychiatric Disorders*; Enna, S. J., Coyle, J. T., Eds.; Mcgraw-Hill Professional: New York, 1998; pp 267−316.

(2) Citron, M. Alzheimer's disease: Strategies for disease modification. *Nat. Rev. Drug Discovery* **2010**, *9*, 387−398.

(3) Hussain, I.; Powell, D.; Howlett, D. R.; Tew, D. G.; Meek, T. D.; Chapman, C.; Gloger, I. S.; Murphy, K. E.; Southan, C. D.; Ryan, D. M.; Smith, T. S.; Simmons, D. L.; Walsh, F. S.; Dingwall, C.; Christie, G. Identification of a novel aspartic protease (Asp 2) as beta-secretase. *Mol. Cell. Neurosci.* **1999**, *14*, 419−427.

(4) Lin, X.; Koelsch, G.; Wu, S.; Downs, D.; Dashti, A.; Tang, J. Human aspartic protease memapsin 2 cleaves the beta-secretase site of beta-amyloid precursor protein. *Proc. Natl. Acad. Sci. U.S.A.* **2000**, *97*, 1456−1460.

(5) Sinha, S.; Anderson, J. P.; Barbour, R.; Basi, G. S.; Caccavello, R.; Davis, D.; Doan, M.; Dovey, H. F.; Frigon, N.; Hong, J.; Jacobson-Croak, K.; Jewett, N.; Keim, P.; Knops, J.; Lieberburg, I.; Power, M.; Tan, H.; Tatsuno, G.; Tung, J.; Schenk, D.; Seubert, P.; Suomensaari, S. M.; Wang, S.; Walker, D.; Zhao, J.; McConlogue, L.; John, V. Purification and cloning of amyloid precursor protein β-secretase from human brain. *Nature* **1999**, *402*, 537−540.

(6) Vassar, R.; Bennett, B. D.; Babu-Khan, S.; Kahn, S.; Mendiaz, E. A.; Denis, P.; Teplow, D. B.; Ross, S.; Amarante, P.; Loeloff, R.; Luo, Y.; Fisher, S.; Fuller, J.; Edenson, S.; Lile, J.; Jarosinski, M. A.; Biere, A. L.; Curran, E.; Burgess, T.; Louis, J. C.; Collins, F.; Treanor, J.; Rogers, G.; Citron, M. Beta-secretase cleavage of Alzheimer's amyloid precursor protein by the transmembrane aspartic protease BACE. *Science* **1999**, *286*, 735−741.

(7) Yan, R.; Bienkowski, M. J.; Shuck, M. E.; Miao, H.; Tory, M. C.; Pauley, A. M.; Brashier, J. R.; Stratman, N. C.; Mathews, W. R.; Buhl, A. E.; Carter, D. B.; Tomasselli, A. G.; Parodi, L. A.; Heinrikson, R. L.; Gurney, M. E. Membrane-anchored aspartyl protease with Alzheimer's disease beta-secretase activity. *Nature* **1999**, *402*, 533−537.

(8) Duff, K.; Eckman, C.; Zehr, C.; Yu, X.; Prada, C. M.; Perez-tur, J.; Hutton, M.; Buee, L.; Harigaya, Y.; Yager, D.; Morgan, D.; Gordon, M. N.; Holcomb, L.; Refolo, L.; Zenk, B.; Hardy, J.; Younkin, S. Increased amyloid-beta42(43) in brains of mice expressing mutant presenilin 1. *Nature* **1996**, *383*, 710−713.

(9) Scheuner, D.; Eckman, C.; Jensen, M.; Song, X.; Citron, M.; Suzuki, N.; Bird, T. D.; Hardy, J.; Hutton, M.; Kukull, W.; Larson, E.; Levy-Lahad, E.; Viitanen, M.; Peskind, E.; Poorkaj, P.; Schellenberg, G.; Tanzi, R.; Wasco, W.; Lannfelt, L.; Selkoe, D.; Younkin, S. Secreted amyloid beta-protein similar to that in the senile plaques of Alzheimer's disease is increased in vivo by the presenilin 1 and 2 and APP mutations linked to familial Alzheimer's disease. *Nat. Med.* **1996**, *2*, 864−870.

(10) Huse, J. T.; Pijak, D. S.; Leslie, G. J.; Lee, V. M.; Doms, R. W. Maturation and endosomal targeting of beta-site amyloid precursor protein-cleaving enzyme. The Alzheimer's disease beta-secretase. *J. Biol. Chem.* **2000**, *275*, 33729−33737.

(11) Liu, K.; Doms, R. W.; Lee, V. M. Glu11 site cleavage and N-terminally truncated A beta production upon BACE overexpression. *Biochemistry* **2002**, *41*, 3128−3136.

(12) Lee, E. B.; Skovronsky, D. M.; Abtahian, F.; Doms, R. W.; Lee, V. M. Secretion and intracellular generation of truncated Abeta in beta-site amyloid-beta precursor protein-cleaving enzyme expressing human neurons. *J. Biol. Chem.* **2003**, *278*, 4458−4466.

(13) Zhou, L.; Brouwers, N.; Benilova, I.; Vandersteen, A.; Mercken, M.; Van Laere, K.; Van Damme, P.; Demedts, D.; Van Leuven, F.; Sleegers, K.; Broersen, K.; Van Broeckhoven, C.; Vandenberghe, R.; De Strooper, B. Amyloid precursor protein mutation E682K at the alternative β-secretase cleavage β′-site increases Aβ generation. *EMBO Mol. Med.* **2011**, *3*, 291−302.

(14) Oster-Granite, M. L.; McPhie, D. L.; Greenan, J.; Neve, R. L. Age-dependent neuronal and synaptic degeneration in mice transgenic for the C terminus of the amyloid precursor protein. *J. Neurosci.* **1996**, *16*, 6732−6741.

(15) Cai, H.; Wang, Y.; McCarthy, D.; Wen, H.; Borchelt, D. R.; Price, D. L.; Wong, P. C. BACE1 is the major beta-secretase for generation of Abeta peptides by neurons. *Nat. Neurosci.* **2001**, *4*, 233−234.

(16) Luo, Y.; Bolon, B.; Kahn, S.; Bennett, B. D.; Babu-Khan, S.; Denis, P.; Fan, W.; Kha, H.; Zhang, J.; Gong, Y.; Martin, L.; Louis, J. C.; Yan, Q.; Richards, W. G.; Citron, M.; Vassar, R. Mice deficient in BACE1, the Alzheimer's beta-secretase, have normal phenotype and abolished beta-amyloid generation. *Nat. Neurosci.* **2001**, *4*, 231−232.

(17) Roberds, S. L.; Anderson, J.; Basi, G.; Bienkowski, M. J.; Branstetter, D. G.; Chen, K. S.; Freedman, S. B.; Frigon, N. L.; Games, D.; Hu, K.; Johnson-Wood, K.; Kappenman, K. E.; Kawabe, T. T.; Kola, I.; Kuehn, R.; Lee, M.; Liu, W.; Motter, R.; Nichols, N. F.; Power, M.; Robertson, D. W.; Schenk, D.; Schoor, M.; Shopp, G. M.; Shuck, M. E.; Sinha, S.; Svensson, K. A.; Tatsuno, G.; Tintrup, H.; Wijsman, J.; Wright, S.; McConlogue, L. BACE knockout mice are healthy despite lacking the primary beta-secretase activity in brain: implications for Alzheimer's disease therapeutics. *Hum. Mol. Genet.* **2001**, *10*, 1317−1324.

(18) Dominguez, D.; Tournoy, J.; Hartmann, D.; Huth, T.; Cryns, K.; Deforce, S.; Serneels, L.; Camacho, I. E.; Marjaux, E.; Craessaerts, K.; Roebroek, A. J.; Schwake, M.; D'Hooge, R.; Bach, P.; Kalinke, U.; Moechars, D.; Alzheimer, C.; Reiss, K.; Saftig, P.; de Strooper, B. Phenotypic and biochemical analyses of BACE1- and BACE2-deficient Mice. *J. Biol. Chem.* **2005**, *280*, 30797−30806.

(19) Rabe, S.; Reichwald, J.; Ammaturo, D.; de Strooper, B.; Saftig, P.; Neumann, U.; Staufenbiel, M. The Swedish APP mutation alters the effect of genetically reduced BACE1 expression on the APP processing. *J. Neurochem.* **2011**, *119*, 231−239.

(20) Pastorino, L.; Ikin, A. F.; Lamprianou, S.; Vacaresse, N.; Revelli, J. P.; Platt, K.; Paganetti, P.; Mathews, P. M.; Harroch, S.; Buxbaum, J. D. BACE (beta-secretase) modulates the processing of APLP2 in vivo. *Mol. Cell. Neurosci.* **2004**, *25*, 642−649.

(21) Laird, F. M.; Cai, H.; Savonenko, A. V.; Farah, M. H.; He, K.; Melnikova, T.; Wen, H.; Chiang, H. C.; Xu, G.; Koliatsos, V. E.; Borchelt, D. R.; Price, D. L.; Lee, H. K.; Wong, P. C. BACE1, a major determinant of selective vulnerability of the brain to amyloid-beta amyloidogenesis, is essential for cognitive, emotional, and synaptic functions. *J. Neurosci.* **2005**, *25*, 11693−11709.

(22) McConlogue, L.; Buttini, M.; Anderson, J. P.; Brigham, E. F.; Chen, K. S.; Freedman, S. B.; Games, D.; Johnson-Wood, K.; Lee, M.; Zeller, M.; Liu, W.; Motter, R.; Sinha, S. Partial reduction of BACE1 has dramatic effects on Alzheimer plaque and synaptic pathology in APP Transgenic Mice. *J. Biol. Chem.* **2007**, *282*, 26326−26334.

(23) Sankaranarayanan, S.; Price, E. A.; Wu, G.; Crouthamel, M. C.; Shi, X. P.; Tugusheva, K.; Tyler, K. X.; Kahana, J.; Ellis, J.; Jin, L.; Steele, T.; Stachel, S.; Coburn, C.; Simon, A. J. In vivo beta-secretase 1 inhibition leads to brain Abeta lowering and increased alpha-secretase processing of amyloid precursor protein without effect on neuregulin-1. *J. Pharmacol. Exp. Ther.* **2008**, *324*, 957−969.

(24) Hu, X.; Hicks, C. W.; He, W.; Wong, P.; Macklin, W. B.; Trapp, B. D.; Yan, R. Bace1 modulates myelination in the central and peripheral nervous system. *Nat. Neurosci.* **2006**, *9*, 1520−1525.

(25) Willem, M.; Garratt, A. N.; Novak, B.; Citron, M.; Kaufmann, S.; Rittger, A.; DeStrooper, B.; Saftig, P.; Birchmeier, C.; Haass, C. Control of peripheral nerve myelination by the beta-secretase BACE1. *Science* **2006**, *314*, 664−666.

(26) Hu, X.; He, W.; Diaconu, C.; Tang, X.; Kidd, G. J.; Macklin, W. B.; Trapp, B. D.; Yan, R. Genetic deletion of BACE1 in mice affects remyelination of sciatic nerves. *FASEB J.* **2008**, *22*, 2970−2980.

(27) Farah, M. H.; Pan, B. H.; Hoffman, P. N.; Ferraris, D.; Tsukamoto, T.; Nguyen, T.; Wong, P. C.; Price, D. L.; Slusher, B. S.; Griffin, J. W. Reduced BACE1 activity enhances clearance of myelin debris and regeneration of axons in the injured peripheral nervous system. *J. Neurosci.* **2011**, *31*, 5744−5754.

(28) Wang, H.; Song, L.; Laird, F.; Wong, P. C.; Lee, H. K. BACE1 knock-outs display deficits in activity-dependent potentiation of synaptic transmission at mossy fiber to CA3 synapses in the hippocampus. *J. Neurosci.* **2008**, *28*, 8677−8681.

(29) Hu, X. Y.; Zhou, X. D.; He, W. X.; Yang, J.; Xiong, W. C.; Wong, P.; Wilson, C. G.; Yan, R. Q. BACE1 deficiency causes altered neuronal activity and neurodegeneration. *J. Neurosci.* **2010**, *30*, 8819−8829.

(30) (a) Wager, T. T.; Villalobos, A.; Verhoest, P. R.; Hou, X.; Shaffer, C. L. Strategies to optimize the brain availability of central nervous system drug candidates. *Expert Opin. Drug Discovery* **2011**, *6*, 371−381. (b) Wager, T. T.; Chandrasekaran, R. Y.; Hou, X.; Troutman, M. D.; Verhoest, P. R.; Villalobos, A.; Will, Y. Defining desirable central nervous system drug space through the alignment of molecular properties, in vitro ADME, and safety attributes. *ACS Chem. Neurosci.* **2010**, *1*, 420−434. (c) Pardridge, W. M. Blood-brain barrier delivery. *Drug Discovery Today* **2007**, *12*, 54−61. (d) Hitchcock, S. A.; Pennington, L. D. Structure-brain exposure relationships. *J. Med. Chem.* **2006**, *49*, 7559−7583. (e) Clark, D. E. Rapid calculation of polar molecular surface area and its application to the prediction of transport phenomena. 2. Prediction of blood-brain barrier penetration. *J. Pharm. Sci.* **1999**, *88*, 815−821.

(31) Ghosh, A. K.; Shin, D.; Downs, D.; Koelsch, G.; Lin, X.; Ermolieff, J.; Tang, J. Design of potent inhibitors for human brain Memapsin 2 (Beta-Secretase). *J. Am. Chem. Soc.* **2000**, *122*, 3522−3523.

(32) Maillaird, M.; Hom, R.; Gailunas, A.; Jagodzinska, B.; Fang, L. Y.; John, V.; Freskos, J. N.; Pulley, S. R.; Beck, J. P.; Tenbrink, R. E. Preparation of substituted amines to treat Alzheimer's disease. Patent WO2002002512, 2002.

(33) Maillard, M.; Baldwin, E. T.; Beck, J. T.; Hughes, R.; John, V.; Pulley, S. R.; Tenbrink, R. Preparation of ring-containing N-acetyl 2-hydroxy-1,3-diaminoalkanes as β-secretase inhibitors for treating Alzheimer's disease and other diseases characterized by deposition of Aβ-peptide. Patent WO2004024081, 2004.

(34) Truong, A. P.; Probst, G. D.; Aquino, J.; Fang, L.; Brogley, L.; Sealy, J. M.; Hom, R. K.; Tucker, J. A.; John, V.; Tung, J. S.; Pleiss, M. A.; Konradi, A. W.; Sham, H. L.; Dappen, M. S.; Tóth, G.; Yao, N.; Brecht, E.; Pan, H.; Artis, D. R.; Ruslim, L.; Bova, M. P.; Sinha, S.; Yednock, T. A.; Zmolek, W.; Quinn, K. P.; Sauer, J. M. Improving the permeability of the hydroxyethylamine BACE-1 inhibitors: Structure-activity relationship of P2′ substituents. *Bioorg. Med. Chem. Lett.* **2010**, *20*, 4789−4794.

(35) Auberson, Y.; Glatthar, R.; Salter, R.; Simic, O.; Tintelnot-Blomley, M. Preparation of substituted spirocyclic lactams as inhibitors of proteinase BACE1. Patent WO2005035535, 2005.

(36) (a) Seelig, A.; Landwojtowicz, E. Structure-activity relationship of P-glycoprotein substrates and modifiers. *Eur. J. Pharm. Sci.* **2000**, *12*, 31−40. (b) Seelig, A. A general pattern for substrate recognition by P-glycoprotein. *Eur. J. Biochem.* **1998**, *251*, 252−261. (c) Cianchetta, G.; Singleton, R. W.; Zhang, M.; Wildgoose, M.; Giesing, D.; Fravolini, A.; Cruciani, G.; Vaz, R. J. A pharmacophore hypothesis for P-glycoprotein substrate recognition using GRIND-based 3D-QSAR. *J. Med. Chem.* **2005**, *48*, 2927−2935. (d) Didziapetris, R.; Japertas, P.; Avdeef, A.; Petrauskas, A. Classification analysis of P-glycoprotein substrate specificity. *J. Drug Target* **2003**, *11*, 391−406.

(37) For recent reviews discussing hydroxyethylamine (HEA) and nontransition state isostere-based inhibitors of BACE1, see (a) Silvestri, R. Boom in the development of non-peptidic beta-secretase (BACE1) inhibitors for the treatment of Alzheimer's disease. *Med. Res. Rev.* **2009**, *29*, 295−338. (b) Hamada, Y.; Kiso, Y. Recent progress in the drug discovery of non-peptidic BACE1 inhibitors. *Expert Opin. Drug Discovery* **2009**, *4*, 391−416. (c) Stachel, S. J. Progress toward the development of a viable BACE-1 inhibitor. *Drug Dev. Res.* **2009**, *70*, 101−110.

(38) For recent papers discussing HEA BACE1 inhibitors, see (a) Maillard, M. C.; Hom, R. K.; Benson, T. E.; Moon, J. B.; Mamo, S.; Bienkowski, M.; Tomasselli, A. G.; Woods, D. D.; Prince, D. B.; Paddock, D. J.; Emmons, T. L.; Tucker, J. A.; Dappen, M. S.; Brogley, L.; Thorsett, E. D.; Jewett, N.; Sinha, S.; John, V. Design, synthesis, and crystal structure of hydroxyethyl secondary amine-based peptidomimetic inhibitors of human beta-secretase. *J. Med. Chem.* **2007**, *50*, 776−781. (b) Charrier, N.; Clarke, B.; Cutler, L.; Demont, E.; Dingwall, C.; Dunsdon, R.; East, P.; Hawkins, J.; Howes, C.; Hussain, I.; Jeffrey, P.; Maile, G.; Matico, R.; Mosley, J.; Naylor, A.; O'Brien, A.; Redshaw, S.; Rowland, P.; Soleil, V.; Smith, K. J.; Sweitzer, S.; Theobald, P.; Vesey, D.; Walter, D. S.; Wayne, G. Second generation of hydroxyethylamine BACE-1 inhibitors: Optimizing potency and oral bioavailability. *J. Med. Chem.* **2008**, *51*, 3313−3317. (c) Iserloh, U.; Wu, Y.; Cumming, J. N.; Pan, J.; Wang, L. Y.; Stamford, A. W.; Kennedy, M. E.; Kuvelkar, R.; Chen, X.; Parker, E. M.; Strickland, C.; Voigt, J. Potent pyrrolidine- and piperidine-based BACE-1 inhibitors. *Bioorg. Med. Chem. Lett.* **2008**, *18*, 414−417. (d) Iserloh, U.; Pan, J.; Stamford, A. W.; Kennedy, M. E.; Zhang, Q.; Zhang, L.; Parker, E. M.; McHugh, N. A.; Favreau, L.; Strickland, C.; Voigt, J. Discovery of an orally efficacious 4-phenoxypyrrolidine-based BACE-1 inhibitor. *Bioorg. Med. Chem. Lett.* **2008**, *18*, 418−422. (e) Clarke, B.; Demont, E.; Dingwall, C.; Dunsdon, R.; Faller, A.; Hawkins, J.; Hussain, I.; MacPherson, D.; Maile, G.; Matico, R.; Milner, P.; Mosley, J.; Naylor, A.; O'Brien, A.; Redshaw, S.; Riddell, D.; Rowland, P.; Soleil, V.; Smith, K. J.; Stanway, S.; Stemp, G.; Sweitzer, S.; Theobald, P.; Vesey, D.; Walter, D. S.; Ward, J.; Wayne, G. BACE-1 inhibitors part 2: Identification of hydroxy ethylamines (HEAs) with reduced peptidic character. *Bioorg. Med. Chem. Lett.* **2008**, *18*, 1017−1021. (f) Beswick, P.; Charrier, N.; Clarke, B.; Demont, E.; Dingwall, C.; Dunsdon, R.; Faller, A.; Gleave, R.; Hawkins, J.; Hussain, I.; Johnson, C. N.; MacPherson, D.; Maile, G.; Matico, R.; Milner, P.; Mosley, J.; Naylor, A.; O'Brien, A.; Redshaw, S.; Riddell, D.; Rowland, P.; Skidmore, J.; Soleil, V.; Smith, K. J.; Stanway, S.; Stemp, G.; Stuart, A.; Sweitzer, S.; Theobald, P.; Vesey, D.; Walter, D. S.; Ward, J.; Wayne, G. BACE-1 inhibitors part 3: Identification of hydroxy ethylamines (HEAs) with nanomolar potency in cells. *Bioorg. Med. Chem. Lett.* **2008**, *18*, 1022−1026. (g) Park, H.; Min, K.; Kwak, H.-S.; Koo, K. D.; Lim, D.; Seo, S.-W.; Choi, J.-U.; Platt, B.; Choi, D.-Y. Synthesis, SAR, and X-ray structure of human BACE-1 inhibitors with cyclic urea derivatives. *Bioorg. Med. Chem. Lett.* **2008**, *18*, 2900−2904. (h) Cumming, J. N.; Le, T. X.; Babu, S.; Carroll, C.; Chen, X.; Favreau, L.; Gaspari, P.; Guo, T.; Hobbs, D. W.; Huang, Y.; Iserloh, U.; Kennedy, M. E.; Kuvelkar, R.; Li, G.; Lowrie, J.; McHugh, N. A.; Ozgur, L.; Pan, J.; Parker, E. M.; Saionz, K.; Stamford, A. W.; Strickland, C.; Tadesse, D.; Voigt, J.; Wang, L.; Wu, Y.; Zhang, L.; Zhang, Q. Rational design of novel, potent piperazinone and

imidazolidinone BACE-1 inhibitors. *Bioorg. Med. Chem. Lett.* **2008**, *18*, 3236−3241. (i) Chirapu, S. R.; Pachaiyappan, B.; Nural, H. F.; Cheng, X.; Yuan, H.; Lankin, D. C.; Abdul-Hay, S. O.; Thatcher, G. R.; Shen, Y.; Kozikowski, A. P.; Petukhov, P. A. Molecular modeling, synthesis, and activity studies of novel biaryl and fused-ring BACE1 inhibitors. *Bioorg. Med. Chem. Lett.* **2009**, *19*, 264−274. (j) Charrier, N.; Clarke, B.; Cutler, L.; Demont, E.; Dingwall, C.; Dunsdon, R.; Hawkins, J.; Howes, C.; Hubbard, J.; Hussain, I.; Maile, G.; Matico, R.; Mosley, J.; Naylor, A.; O'Brien, A.; Redshaw, S.; Rowland, P.; Soleil, V.; Smith, K. J.; Sweitzer, S.; Theobald, P.; Vesey, D.; Walter, D. S.; Wayne, G. Second generation of BACE-1 inhibitors. Part 1: The need for improved pharmacokinetics. *Bioorg. Med. Chem. Lett.* **2009**, *19*, 3664−3668. (k) Charrier, N.; Clarke, B.; Demont, E.; Dingwall, C.; Dunsdon, R.; Hawkins, J.; Hubbard, J.; Hussain, I.; Maile, G.; Matico, R.; Mosley, J.; Naylor, A.; O'Brien, A.; Redshaw, S.; Rowland, P.; Soleil, V.; Smith, K. J.; Sweitzer, S.; Theobald, P.; Vesey, D.; Walter, D. S.; Wayne, G. Second generation of BACE-1 inhibitors part 2: Optimisation of the non-prime side substituent. *Bioorg. Med. Chem. Lett.* **2009**, *19*, 3669−3673. (l) Charrier, N.; Clarke, B.; Cutler, L.; Demont, E.; Dingwall, C.; Dunsdon, R.; Hawkins, J.; Howes, C; Hubbard, J.; Hussain, I.; Maile, G.; Matico, R.; Mosley, J.; Naylor, A.; O'Brien, A.; Redshaw, S.; Rowland, P.; Soleil, V.; Smith, K. J.; Sweitzer, S.; Theobald, P.; Vesey, D.; Walter, D. S.; Wayne, G. Second generation of BACE-1 inhibitors part 3: Towards non-hydroxyethylamine transition state mimetics. *Bioorg. Med. Chem. Lett.* **2009**, *19*, 3674−3678. (m) Sealy, J. M.; Truong, A. P.; Tso, L.; Probst, G. D.; Aquino, J.; Hom, R. K.; Jagodzinska, B. M.; Dressen, D.; Wone, D. W.; Brogley, L.; John, V.; Tung, J. S.; Pleiss, M. A.; Tucker, J. A.; Konradi, A. W.; Dappen, M. S.; Tóth, G.; Pan, H.; Ruslim, L.; Miller, J.; Bova, M. P.; Sinha, S.; Quinn, K. P.; Sauer, J.-M. Design and synthesis of cell potent BACE-1 inhibitors: structure-activity relationship of P1′ substituents. *Bioorg. Med. Chem. Lett.* **2009**, *19*, 6386−6391. (n) Truong, A. P.; Probst, G. D.; Aquino, J.; Fang, L.; Brogley, L.; Sealy, J. M.; Hom, R. K.; Tucker, J. A.; John, V.; Tung, J. S.; Pleiss, M. A.; Konradi, A. W.; Sham, H. L.; Dappen, M. S.; Tóth, G.; Yao, N.; Brecht, E.; Pan, H.; Artis, D. R.; Ruslim, L.; Bova, M. P.; Sinha, S.; Yednock, T. A.; Zmolek, W.; Quinn, K. P.; Sauer, J. M. Improving the permeability of the hydroxyethylamine BACE-1 inhibitors: Structure-activity relationship of P2′ substituents. *Bioorg. Med. Chem. Lett.* **2010**, *20*, 4789−4794. (o) Probst, G. D.; Bowers, S.; Sealy, J. M.; Stupi, B.; Dressen, D.; Jagodzinska, B. M.; Aquino, J.; Gailunas, A.; Truong, A. P.; Tso, L.; Xu, Y.-Z.; Hom, R. K.; John, V.; Tung, J. S.; Pleiss, M. A.; Tucker, J. A.; Konradi, A. W.; Sham, H. L.; Jagodzinski, J.; Toth, G.; Brecht, E.; Yao, N.; Pan, H.; Lin, M.; Artis, D. R.; Ruslim, L.; Bova, M. P.; Sinha, S.; Yednock, T. A.; Gauby, S.; Zmolek, W.; Quinn, K. P.; Sauer, J.-M. Design and synthesis of hydroxyethylamine (HEA) BACE-1 inhibitors: structure-activity relationship of the aryl region. *Bioorg. Med. Chem. Lett.* **2010**, *20*, 6034−6039. (p) Truong, A. P.; Tóth, G.; Probst, G. D.; Sealy, J. M.; Bowers, S.; Wone, D. W.; Dressen, D.; Hom, R. K.; Konradi, A. W.; Sham, H. L.; Wu, J.; Peterson, B. T.; Ruslim, L.; Bova, M. P.; Kholodenko, D.; Motter, R. N.; Bard, F.; Santiago, P.; Ni, H.; Chian, D.; Soriano, F.; Cole, T.; Brigham, E. F.; Wong, K.; Zmolek, W.; Goldbach, E.; Samant, B.; Chen, L.; Zhang, H.; Nakamura, D. F.; Quinn, K. P.; Yednock, T. A.; Sauer, J.-M. Design of an orally efficacious hydroxyethylamine (HEA) BACE-1 inhibitor in a preclinical animal model. *Bioorg. Med. Chem. Lett.* **2010**, *20*, 6231−6236. (q) Marcin, L. R.; Higgins, M. A.; Zusi, F. C; Zhang, Y.; Dee, M. F.; Parker, M. F.; Muckelbauer, J. K.; Camac, D. M.; Morin, P. E.; Ramamurthy, V.; Tebben, A. J.; Lentz, K. A.; Grace, J. E.; Marcinkeviciene, J. A.; Kopcho, L. M.; Burton, C. R.; Barten, D. M.; Toyn, J. H.; Meredith, J. E.; Albright, C. F.; Bronson, J. J.; Macor, J. E.; Thompson, L. A. Synthesis and SAR of indole-and 7-azaindole-1,3-dicarboxamide hydroxyethylamine inhibitors of BACE-1. *Bioorg. Med. Chem. Lett.* **2011**, *21*, 537−541. (r) Boy, K. M.; Guernon, J. M.; Shi, J.; Toyn, J. H.; Meredith, J. E.; Barten, D. M.; Burton, C. R.; Albright, C. F.; Marcinkeviciene, J.; Good, A. C.; Tebben, A. J.; Muckelbauer, J. K.; Camac, D. M.; Lentz, K. A.; Bronson, J. J.; Olson, R. E.; Macor, J. E.; Thompson, L. A. III. Monosubstituted γ-lactam and conformationally constrained 1,3-diaminopropan-2-ol transition-

state isostere inhibitors of $\beta$-secretase (BACE). *Bioorg. Med. Chem. Lett.* **2011**, *21*, 6916−6924.

(39) For recent papers discussing non-HEA BACE1 inhibitors, see (a) Barrow, J. C.; Rittle, K. E.; Ngo, P. L.; Selnick, H. G.; Graham, S. L.; Pitzenberger, S. M.; McGaughey, G. B.; Colussi, D.; Lai, M.-T.; Huang, Q.; Tugusheva, K.; Espeseth, A. S.; Simon, A. J.; Munshi, S. K.; Vacca, J. P. Design and synthesis of 2,3,5-substituted imidazolidin-4-one inhibitors of BACE-1. *ChemMedChem* **2007**, *2*, 995−999. (b) Stanton, M. G.; Stauffer, S. R.; Gregro, A. R.; Steinbeiser, M.; Nantermet, P.; Sankaranarayanan, S.; Price, E. A.; Wu, G.; Crouthamel, M.-C.; Ellis, J.; Lai, M.-T.; Espeseth, A. S.; Shi, X.-P.; Jin, L.; Colussi, D.; Pietrak, B.; Huang, Q.; Xu, M.; Simon, A. J.; Graham, S. L.; Vacca, J. P.; Selnick, H. Discovery of isonicotinamide derived beta-secretase inhibitors: in vivo reduction of beta-amyloid. *J. Med. Chem.* **2007**, *50*, 3431−3433. (c) Baxter, E. W.; Conway, K. A.; Kennis, L.; Bischoff, F.; Mercken, M. H.; Winter, H. L.; Reynolds, C. H.; Tounge, B. A.; Luo, C.; Scott, M. K.; Huang, Y.; Braeken, M.; Pieters, S. M.; Berthelot, D. J.; Masure, S.; Bruinzeel, W. D.; Jordan, A. D.; Parker, M. H.; Boyd, R. E.; Qu, J.; Alexander, R. S.; Brenneman, D. E.; Reitz, A. B. 2-Amino-3,4-dihydroquinazolines as inhibitors of BACE-1 (beta-site APP cleaving enzyme): Use of structure based design to convert a micromolar hit into a nanomolar lead. *J. Med. Chem.* **2007**, *50*, 4261−4264. (d) Barrow, J. C.; Stauffer, S. R.; Rittle, K. E.; Ngo, P. L.; Yang, Z.; Selnick, H. G.; Graham, S. L.; Munshi, S.; McGaughey, G. B.; Holloway, M. K.; Simon, A. J.; Price, E. A.; Sankaranarayanan, S.; Colussi, D.; Tugusheva, K.; Lai, M.-T.; Espeseth, A. S.; Xu, M.; Huang, Q.; Wolfe, A.; Pietrak, B.; Zuck, P.; Levorse, D. A.; Hazuda, D.; Vacca, J. P. Discovery and X-ray crystallographic analysis of a spiropiperidine iminohydantoin inhibitor of beta-secretase. *J. Med. Chem.* **2008**, *51*, 6259−6262. (e) Jennings, L. D.; Cole, D. C.; Stock, J. R.; Sukhdeo, M. N.; Ellingboe, J. W.; Cowling, R.; Jin, G.; Manas, E. S.; Fan, K. Y.; Malamas, M. S.; Harrison, B. L.; Jacobsen, S.; Chopra, R.; Lohse, P. A.; Moore, W. J.; O'Donnell, M.-M.; Hu, Y.; Robichaud, A. J.; Turner, M. J.; Wagner, E.; Bard, J. Acylguanidine inhibitors of beta-secretase: optimization of the pyrrole ring substituents extending into the S1′ substrate binding pocket. *Bioorg. Med. Chem. Lett.* **2008**, *18*, 767−771. (f) Malamas, M. S.; Erdei, J.; Gunawan, I.; Barnes, K.; Johnson, M.; Hui, Y.; Turner, J.; Hu, Y.; Wagner, E.; Fan, K.; Olland, A.; Bard, J.; Robichaud, A. J. Aminoimidazoles as potent and selective human beta-secretase (BACE1) inhibitors. *J. Med. Chem.* **2009**, *52*, 6314−6323. (g) Nantermet, P. G.; Rajapakse, H. A.; Stanton, M. G.; Stauffer, S. R.; Barrow, J. C.; Gregro, A. R.; Moore, K. P.; Steinbeiser, M. A.; Swestock, J.; Selnick, H. G.; Graham, S. L.; McGaughey, G. B.; Colussi, D.; Lai, M.-T.; Sankaranarayanan, S.; Simon, A. J.; Munshi, S.; Cook, J. J.; Holahan, M. A.; Michener, M. S.; Vacca, J. P. Evolution of tertiary carbinamine BACE-1 inhibitors: Abeta reduction in rhesus CSF upon oral dosing. *ChemMedChem* **2009**, *4*, 37−40. (h) Sankaranarayanan, S; Holahan, M. A.; Colussi, D.; Crouthamel, M.-C.; Devanarayan, V.; Ellis, J.; Espeseth, A.; Gates, A. T.; Graham, S. L.; Gregro, A. R.; Hazuda, D.; Hochman, J. H.; Holloway, K.; Jin, L.; Kahana, J.; Lai, M.-T.; Lineberger, J.; McGaughey, G.; Moore, K. P.; Nantermet, P.; Pietrak, B.; Price, E. A.; Rajapakse, H.; Stauffer, S.; Steinbeiser, M. A.; Seabrook, G.; Selnick, H. G.; Shi, X.-P.; Stanton, M. G.; Swestock, J.; Tugusheva, K.; Tyler, K. X.; Vacca, J. P.; Wong, J.; Wu, G.; Xu, M.; Cook, J. J.; Simon, A. J. First demonstration of cerebrospinal fluid and plasma A beta lowering with oral administration of a beta-site amyloid precursor protein-cleaving enzyme 1 inhibitor in nonhuman primates. *J. Pharmacol. Exp. Ther.* **2009**, *328*, 131−140. (i) Zhu, H.; Young, M. B.; Nantermet, P. G.; Graham, S. L.; Colussi, D.; Lai, M.-T.; Pietrak, B.; Price, E. A.; Sankaranarayanan, S.; Shi, X. P.; Tugusheva, K.; Holahan, M. A.; Michener, M. S.; Cook, J. J.; Simon, A; Hazuda, D. J.; Vacca, J. P.; Rajapakse, H. A. Rapid P1 SAR of brain penetrant tertiary carbinamine derived BACE inhibitors. *Bioorg. Med. Chem. Lett.* **2010**, *20*, 1779−1782. (j) Malamas, M. S.; Erdei, J.; Gunawan, I.; Turner, J.; Hu, Y.; Wagner, E.; Fan, K.; Chopra, R.; Olland, A.; Bard, J.; Jacobsen, S.; Magolda, R. L.; Pangalos, M.; Robichaud, A. J. Design and synthesis of 5,5′-disubstituted aminohydantoins as potent and selective human beta-secretase (BACE1) inhibitors. *J. Med. Chem.* **2010**, *53*, 1146−

1158. (k) Malamas, M. S.; Robichaud, A.; Erdei, J.; Quagliato, D.; Solvibile, W.; Zhou, P.; Morris, K.; Turner, J.; Wagner, E.; Fan, K.; Olland, A.; Jacobsen, S.; Reinhart, P.; Riddell, D.; Pangalos, M. Design and synthesis of aminohydantoins as potent and selective human $\beta$-secretase (BACE1) inhibitors with enhanced brain permeability. *Bioorg. Med. Chem. Lett.* **2010**, *20*, 6597−6605.

(40) Fragment-based lead generation: (a) Albert, J. S.; Blomberg, N.; Breeze, A. L.; Brown, A. J.; Burrows, J. N.; Edwards, P. D.; Folmer, R. H.; Geschwindner, S.; Griffen, E. J.; Kenny, P. W.; Nowak, T.; Olsson, L. L.; Sanganee, H.; Shapiro, A. B. An integrated approach to fragment-based lead generation: Philosophy, strategy and case studies from AstraZeneca's drug discovery programmes. *Curr. Top. Med. Chem.* **2007**, *7*, 1600−1629. (b) Geschwindner, S.; Olsson, L.-L.; Albert, J. S.; Deinum, J.; Edwards, P. D.; de Beer, T.; Folmer, R. H.. Discovery of a novel warhead against beta-secretase through fragment-based lead generation. *J. Med. Chem.* **2007**, *50*, 5903−5911. (c) Edwards, P. D.; Albert, J. S.; Sylvester, M.; Aharony, D.; Andisik, D.; Callaghan, O.; Campbell, J. B.; Carr, R. A.; Chessari, G.; Congreve, M.; Frederickson, M.; Folmer, R. H.; Geschwindner, S.; Koether, G.; Kolmodin, K.; Krumrine, J.; Mauger, R. C.; Murray, C. W.; Olsson, L.-L.; Patel, S.; Spear, N.; Tian, G. Application of fragment-based lead generation to the discovery of novel, cyclic amidine beta-secretase inhibitors with nanomolar potency, cellular activity, and high ligand efficiency. *J. Med. Chem.* **2007**, *50*, 5912−5925. (d) Wang, Y.-S.; Strickland, C.; Voigt, J. H.; Kennedy, M. E.; Beyer, B. M.; Senior, M. M.; Smith, E. M.; Nechuta, T. L.; Madison, V. S.; Czarniecki, M.; McKittrick, B. A.; Stamford, A. W.; Parker, E. M.; Hunter, J. C.; Greenlee, W. J.; Wyss, D. F. Application of fragment-based NMR screening, X-ray crystallography, structure-based design, and focused chemical library design to identify novel microM leads for the development of nM BACE-1 (beta-site APP cleaving enzyme 1) inhibitors. *J. Med. Chem.* **2010**, *53*, 942−950. (e) Zhu, Z.; Sun, Z.-Y.; Ye, Y.; Voigt, J.; Strickland, C.; Smith, E. M.; Cumming, J.; Wang, L.; Wong, J.; Wang, Y.-S.; Wyss, D. F.; Chen, X.; Kuvelkar, R.; Kennedy, M. E.; Favreau, L.; Parker, E.; McKittrick, B. A.; Stamford, A.; Czarniecki, M.; Greenlee, W.; Hunter, J. C. Discovery of cyclic acylguanidines as highly potent and selective beta-site amyloid cleaving enzyme (BACE) inhibitors: Part I-inhibitor design and validation. *J. Med. Chem.* **2010**, *53*, 951−965. (f) Madden, J.; Dod, J. R.; Godemann, R.; Kraemer, J.; Smith, M.; Biniszkiewicz, M.; Hallett, D. J.; Barker, J.; Dyekjaer, J. D.; Hesterkamp, T. Fragment-based discovery and optimization of BACE1 inhibitors. *Bioorg. Med. Chem. Lett.* **2010**, *20*, 5329−5333. (g) Cheng, Y.; Judd, T. C.; Bartberger, M. D.; Brown, J.; Chen, K.; Fremeau, R. T.; Hickman, D.; Hitchcock, S. A.; Jordan, B.; Li, V.; Lopez, P.; Louie, S. W.; Luo, Y.; Michelsen, K.; Nixey, T.; Powers, T. S.; Rattan, C.; Sickmier, E. A.; St Jean, D. J. Jr.; Wahl, R. C.; Wen, P. H.; Wood, S. From fragment screening to in vivo efficacy: Optimization of a series of 2-aminoquinolines as potent inhibitors of beta-site amyloid precursor protein cleaving enzyme 1 (BACE1). *J. Med. Chem.* **2011**, *54*, 5836−5857.

(41) Rueeger, H.; Rondeau, J.-M.; McCarthy, C.; Möbitz, H.; Tintelnot-Blomley, M.; Neumann, U.; Desrayaud, S. Structure based design, synthesis and SAR of cyclic hydroxyethylamine (HEA) BACE-1 inhibitors. *Bioorg. Med. Chem. Lett.* **2011**, *21*, 1942−1947.

(42) Shacka, J. J.; Roth, K. A. Cathepsin D Deficiency and NCL/Batten disease: There's More to Death than Apoptosis. *Autophagy* **2007**, *3*, 474−476.

(43) (a) Mahar Doan, K. M.; Humphreys, J. E.; Webster, L. O.; Wring, S. A.; Shampine, L. J.; Serabjit-Singh, C. J.; Adkison, K. K.; Polli, J. W. Passive permeability and P-glycoprotein-mediated efflux differentiate central nervous system (CNS) and non-CNS marketed drugs. *J. Pharmacol. Exp. Ther.* **2002**, *303*, 1029−1037. (b) Wang, Q.; Rager, J. D.; Weinstein, K.; Kardos, P. S.; Dobson, G. L.; Li, J.; Hidalgo, I. J. Evaluation of the MDR-MDCK cell line as a permeability screen for the blood-brain barrier. *Int. J. Pharm.* **2005**, *288*, 349−359. (c) Di, L.; Kerns, E. H.; Carter, G. T. Strategies to assess blood-brain barrier penetration. *Expert Opin. Drug Discovery* **2008**, *3*, 677−687. (d) Read, K. D.; Braggio, S. Assessing brain free fraction in early drug discovery. *Expert Opin. Drug Metab. Toxicol.* **2010**, *6*, 337−344.

(44) (a) Didziapetris, R.; Japertas, P.; Avdeef, A.; Petrauskas, A. Classification analysis of P-glycoprotein substrate specificity. *J. Drug Targeting* **2003**, *11*, 391−406. (b) Norinder, U; Haeberlein, M. Computational approaches to the prediction of the blood-brain distribution. *Adv. Drug Delivery Rev.* **2002**, *54*, 291−313.

(45) Aronov, A. M. Ligand structural aspects of hERG channel blockade. *Curr. Top. Med. Chem.* **2008**, *8*, 1113−1127.

(46) Limongelli, V.; Marinelli, L.; Cosconati, S.; Braun, H. A.; Schmidt, B.; Novellino, E. Ensemble-docking approach on BACE-1: Pharmacophore perception and guidelines for drug design. *Chem-MedChem* **2007**, *2*, 667−678.

(47) McMartin, C.; Bohacek, R. S. QXP: Powerful, rapid computer algorithms for structure-based drug design. *J. Comput.-Aided Mol. Des.* **1997**, *11*, 333−344.

(48) York, C.; Prakash, G. K. S.; Wang, Q.; Olah, G. A. Synthetic methods and reactions. 189. Novel preparation of gem-difluorides from ketoximes with nitrosonium tetrafluoroborate and pyridinium polyhydrogen fluoride. *Synlett* **1994**, 425−426.

(49) Bunch, J. E.; Bumgardner, C. L. Aryl(trifluoromethyl)acetylenes. *J. Fluorine Chem.* **1987**, *36*, 313−317.

(50) Takahashi, O.; Furuhashi, K.; Fukumasa, M.; Hirai, T. Trifluoropropene oxide as a trifluoromethyl source. Preparation of optically active alcohols. *Tetrahedron Lett.* **1990**, *31*, 7031−7034.

(51) (a) Saiakhov, R. D.; Klopman, G. MultiCASE Expert Systems and the REACH Initiative. *Toxicol. Mech. Methods* **2008**, *18*, 159−175. (b) MCASE (MC4PC V. 1.9, ANK module): Biophore for mutagenicity was found (located in aromatic amine moiety). However, the calculated activity of these biophores was reduced due to an inactivating modulator and a deactivating fragment. Thus, the compounds are expected to be inactive in the Ames test.

(52) Dalvit, C.; Vulpetti, A. Fluorine-protein interactions and $^{19}$F NMR isotropic chemical shifts: An empirical correlation with implications for drug design. *ChemMedChem* **2011**, *6*, 104−114.

(53) Davies, B.; Morris, T. Physiological parameters in laboratory animals and humans. *Pharm. Res.* **1993**, *10*, 1093−1095.

(54) Hanessian, S.; Yun, H.; Hou, Y.; Yang, G.; Bayrakdarian, M.; Therrien, E.; Moitessier, N.; Roggo, S.; Veenstra, S.; Tintelnot-Blomley, M.; Rondeau, J.-M.; Ostermeier, C.; Strauss, A.; Ramage, P.; Paganetti, P.; Neumann, U.; Betschart, C. Structure-based design, synthesis, and memapsin 2 (BACE) inhibitory activity of carbocyclic and heterocyclic peptidomimetics. *J. Med. Chem.* **2005**, *48*, 5175−5190.

(55) Otwinowski, Z.; Minor, W. Processing of X-ray diffraction data collected in oscillation mode. *Methods Enzymol.* **1997**, *276*, 407−426.

(56) Kabsch, W. Automatic processing of rotation diffraction data from crystals of initially unknown symmetry and cell constants. *J. Appl. Crystallogr.* **1993**, *26*, 795−800.

(57) Kroemer, M.; Dreyer, M. K.; Wendt, K. U. APRV − a program for automated data processing, refinement and visualization. *Acta Crystallogr., Sect. D: Biol. Crystallogr.* **2004**, *60*, 1679−1682.

(58) Brünger, A. T.; Adams, P. D.; Clore, G. M.; DeLano, W. L.; Gros, P.; Grosse-Kunstleve, R. W.; Jiang, J.-S.; Kuszewski, J.; Nilges, M.; Pannu, N. S.; Read, R. J.; Rice, L. M.; Simonson, T.; Warren, G. L. Crystallography & NMR System: A new software suite for macromolecular structure determination. *Acta Crystallogr., Sect. D: Biol. Crystallogr.* **1998**, *54*, 905−921.

(59) Emsley, P.; Lohkamp, B.; Scott, W.; Cowtan, K. Features and development of Coot. *Acta Crystallogr., Sect. D: Biol. Crystallogr.* **2010**, *66*, 486−501.